

TenExp: Mixture-of-Experts-Based Tensor Decomposition Structure Search Framework

Ting-Wei Zhou, Xi-Le Zhao*, Sheng Liu, Wei-Hao Wu, Yu-Bang Zheng, Deyu Meng

Abstract—Recently, tensor decompositions continue to emerge and receive increasing attention. Selecting a suitable tensor decomposition to exactly capture the low-rank structures behind the data is at the heart of the tensor decomposition field, which remains a challenging and relatively under-explored problem. Current tensor decomposition structure search methods are still confined by a fixed factor-interaction family (e.g., tensor contraction) and cannot deliver the mixture of decompositions. To address this problem, we elaborately design a mixture-of-experts-based tensor decomposition structure search framework (termed as TenExp), which allows us to dynamically select and activate suitable tensor decompositions in an unsupervised fashion. This framework enjoys two unique advantages over the state-of-the-art tensor decomposition structure search methods. Firstly, TenExp can provide a suitable single decomposition beyond a fixed factor-interaction family. Secondly, TenExp can deliver a suitable mixture of decompositions beyond a single decomposition. Theoretically, we also provide the approximation error bound of TenExp, which reveals the approximation capability of TenExp. Extensive experiments on both synthetic and realistic datasets demonstrate the superiority of the proposed TenExp compared to the state-of-the-art tensor decomposition-based methods.

Index Terms—Tensor decomposition, tensor decomposition structure search, multi-dimensional data recovery.

I. INTRODUCTION

Recent technological advancements have led to a rapid surge in diverse types of multi-dimensional data [1]–[6] are increasingly emerging. Mathematically, tensor decomposition is well-suited for representing multi-dimensional data. Due to its capability to preserve the intrinsic multi-dimensional correlations of data, tensor decomposition has garnered substantial attention across multiple domains, including data analysis [7]–[9], machine learning [10], [11], and computer vision [12]–[14].

Tensor decomposition, which decomposes the target tensor into a series of factors (e.g., matrix and tensor) with the factor interaction (i.e., algebraic operation) between them, reveals the intrinsic information behind multi-dimensional data. Different

*Corresponding author: Xi-Le Zhao.

Ting-Wei Zhou, Xi-Le Zhao, Sheng Liu, and Wei-Hao Wu are with the School of Mathematical Sciences/Research Center for Image and Vision Computing, University of Electronic Science and Technology of China, Chengdu, Sichuan 611731, China (e-mail: zhoutingwei2021@163.com; xlzhao122003@163.com; liusheng16@163.com; weihaowu99@163.com).

Yu-Bang Zheng is with the School of Information Science and Technology, Southwest Jiaotong University, Chengdu 611756, China (e-mail: zhengyubang@163.com)

Deyu Meng is with the School of Mathematics and Statistics and Ministry of Education Key Lab of Intelligent Networks and Network Security, Xi’an Jiaotong University, Xi’an, Shaanxi 710049, China, and also with Pazhou Laboratory (Huangpu), Guangzhou, Guangdong 510335, China (e-mail: dymeng@mail.xjtu.edu.cn).

TABLE I: Comparison between classic tensor decomposition structure search methods and our TenExp in terms of search capability and data adaptability.

Characteristic Method	Search Capability						Data Adaptability
	CP	Tucker	TT	TR	FCTN	T-SVD Mixture	
Tucker	✓	✓					
FCTN			✓	✓	✓		
T-SVD						✓	
SVDinsTN			✓	✓	✓		✓
TenExp	✓	✓	✓	✓	✓	✓	✓

factor interactions, including outer product, mode- n product, tensor contraction, and tensor-tensor product (t-product) et al. [15]–[18], can induce different tensor decompositions. The most classical tensor decomposition methods are outer product-induced CANDECOMP/PARAFAC (CP) decomposition [15] and mode- n product-induced Tucker decomposition [16]. It has been demonstrated that CP/Tucker models have been widely adopted to enhance the efficiency of modern algorithms [9], [19]–[21] due to their powerful feature extraction and compression capabilities. A separate category of tensor decomposition is tensor contraction-induced tensor network decomposition [17], which encompasses tensor train (TT) decomposition [22], tensor ring (TR) decomposition [23], and fully-connected tensor network (FCTN) decomposition [24]. These more sophisticated tensor network decompositions have been empirically validated to exhibit robust and generalized capabilities for modeling multi-dimensional data [25]–[28]. Most recently, t-product-induced tensor singular value decomposition (T-SVD) [18] has gained significant attention, mainly due to its close theoretical connection to the matrix singular value decomposition (SVD); see for example [29]–[32]. However, for given data, how to select a suitable tensor decomposition to exactly capture the low-rank structures behind the data remains a challenging and relatively under-explored problem.

Tensor decomposition structure search aims to discover a suitable tensor decomposition structure for compactly representing the given data. The choice of tensor decomposition structure exerts a profound impact on its performance in practical applications. Recently, several pioneer efforts have been proposed [17], [33]–[40]. Most of these approaches adopt a “sampling-evaluation” framework, which necessitates sampling a large pool of candidate structures and performing numerous repeated structure evaluations. Apart from heuristic approaches, the regularity-based method has also been explored for structure optimization [41]. Despite these great efforts, these methods are still confined by a fixed factor-interaction family

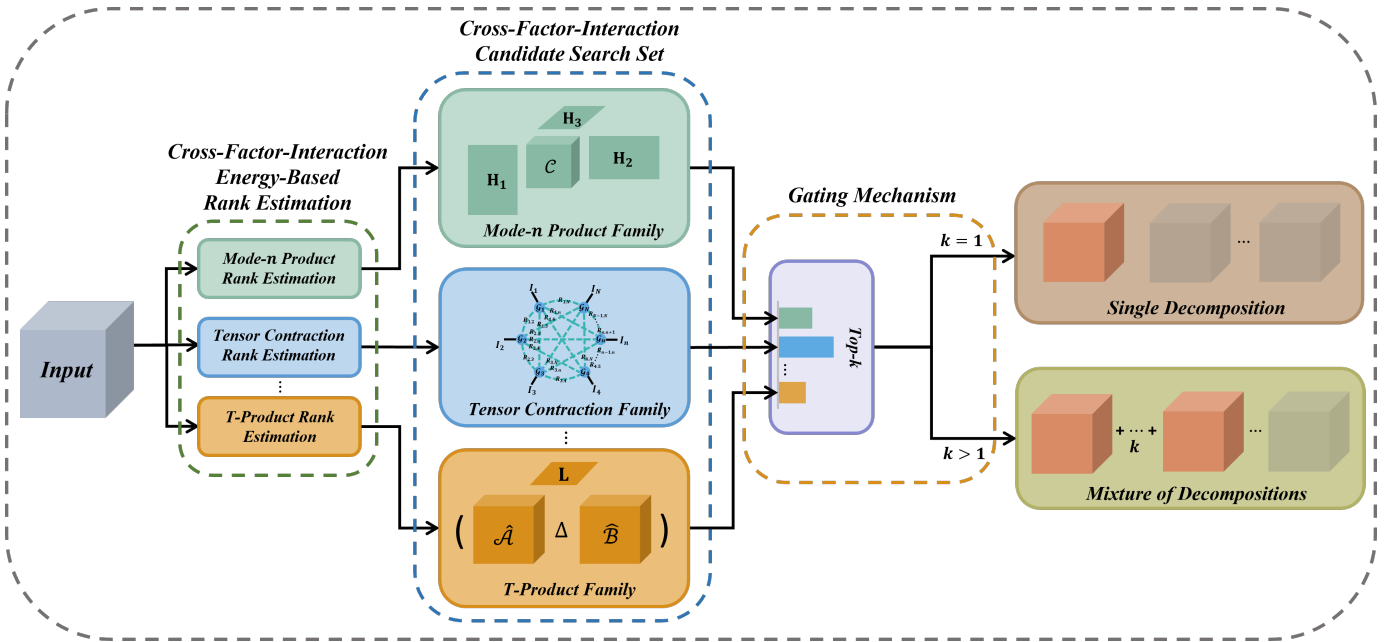


Fig. 1: Diagram of our TenExp. First, we perform the cross-factor-interaction energy-based rank estimation scheme for the input data. Then, the estimated ranks are fed into the cross-factor-interaction candidate search set. Finally, the top- k gating mechanism selects the candidate tensor decompositions, leading to either a single decomposition ($k = 1$) or a mixture of decompositions ($k > 1$).

(e.g., tensor contraction) and fail to search for other factor-interaction families (e.g., t-product). Meanwhile, these methods are only applicable to single decomposition structure search, with no support for delivering the mixture of decompositions; as shown in Table I.

To address these issues, we suggest a mixture-of-experts-based tensor decomposition structure search framework (termed as TenExp); see Fig. 1. Due to the white box nature of tensor decomposition, TenExp can be trained in a fully unsupervised fashion solely from observational data, which can handle tensors of different orders and sizes, eliminating the need for any extra pre-constructed datasets. In summary, the main contributions of this work are as follows:

- To address the challenging and relatively under-explored problem of selecting a suitable tensor decomposition to exactly capture the low-rank structures behind the data, we elaborately design a mixture-of-experts-based tensor decomposition structure search framework, which allows us to dynamically select and activate suitable tensor decompositions in an unsupervised fashion. This framework enjoys two unique advantages over the state-of-the-art tensor decomposition structure search methods. Firstly, TenExp can provide a suitable single decomposition beyond a fixed factor-interaction family. Secondly, TenExp can deliver a suitable mixture of decompositions beyond a single decomposition.
- To provide a general cross-factor-interaction candidate search set, we first systematically review tensor decompositions. Based on the cross-factor-interaction candidate search set, we suggest a unified cross-factor-interaction energy-based rank estimation scheme for different tensor

decompositions. Theoretically, we provide the approximation error bound of TenExp to reveal the approximation capability of TenExp.

- Extensive experiments on both synthetic datasets and realistic datasets consistently demonstrate that the proposed TenExp outperforms the state-of-the-art tensor decomposition-based methods.

The remainder of this paper is organized as follows: Section II provides a comprehensive review of related work on tensor decomposition and tensor decomposition structure search. Section III introduces the necessary notations and preliminary concepts for tensor decomposition. Section IV details the proposed TenExp and presents an unsupervised multidimensional data recovery model. Section V reports the results of extensive experiments on synthetic and realistic datasets. Section VI discusses the experimental findings and insights. Finally, Section VII concludes this work and summarizes its main contributions.

II. RELATED WORK

A. Tensor Decomposition

Most realistic data (e.g., multispectral images (MSIs), color videos, and light field data) inherently exhibit low-rank structures. Consequently, low-rank decomposition of matrices and tensors has become a widely studied topic in data processing. Unlike matrices, the rank definition of high-order tensors lacks a unified formulation. So far, many tensor ranks based on different factor interactions (e.g., outer product, mode- n product, tensor contraction, and t-product) have been proposed. The most classical tensor ranks include the outer product-based CP rank (defined as the minimum number of rank-

one tensors required for decomposition) [15] and the mode- n product-based Tucker rank (defined by the rank of tensor unfolding matrices) [16]. It has been demonstrated that solving low-CP-rank or low-Tucker-rank optimization problems yields effective low-rank representation of multi-dimensional data [9], [19]. Moreover, low-Tucker/CP-rank models have been widely adopted to enhance the efficiency of modern deep learning algorithms [20], [21] due to their powerful feature extraction and compression capabilities. Another category of tensor contraction-based tensor ranks is derived from tensor network decomposition [17], such as TT rank [22], TR rank [23], and FCTN rank [24]. These relatively complex rank-based decompositions have powerful representation capability for multi-dimensional data modeling [25]–[28]. More recently, the t-product-based tensor tubal-rank [18], which is rooted in T-SVD, has garnered significant attention, primarily due to its close connection to the matrix SVD definition. Additionally, the effectiveness of tubal-rank minimization has been validated across various signal processing tasks [29]–[32].

However, for given data, how to select a suitable tensor decomposition to exactly capture the low-rank structures behind the data remains a challenging and relatively under-explored problem.

B. Tensor Decomposition Structure Search

Tensor decomposition structure search aims to discover a suitable tensor decomposition structure for compactly representing the given data. Pioneer approaches [17], [33]–[40] adopt a “sampling-evaluation” framework, which relies on heuristic search algorithms to sample candidate structures, then evaluate each candidate individually. For instance, Hashemizadeh *et al.* [34] proposed a greedy algorithm-based method that starts from a rank-one tensor and sequentially identifies the most promising tensor network edges to incrementally increase rank. Li *et al.* [17] developed a genetic meta-algorithm to search for optimal structure in Hamming space; they also proposed a local enumeration algorithm [36] to alternately update each structure-related variable. Apart from heuristic approaches, the regularity-based method has also been explored for structure search. Zheng *et al.* [41] proposed the SVD-inspired tensor network decomposition (SVDinsTN) to address tensor network structure search via regularized modeling, which greatly reduces computational costs.

Despite these great efforts, these methods are still confined by a fixed factor-interaction family (e.g., tensor contraction) and fail to search for other factor-interaction families (e.g., t-product). Meanwhile, these methods are only applicable to single decomposition structure search, with no support for delivering the mixture of decompositions.

III. NOTATIONS AND PRELIMINARIES

A. Notations

Scalars, vectors, matrices, and tensors are denoted by x , \mathbf{x} , \mathbf{X} , and \mathcal{X} , respectively. For a vector $\mathbf{x} \in \mathbb{R}^I$, we use $\mathbf{x}(n) \in \mathbb{R}$ to denote the n -th element of \mathbf{x} . Meanwhile, for an N th-order tensor $\mathcal{X} \in \mathbb{R}^{I_1 \times I_2 \times \dots \times I_N}$, we use $\mathcal{X}(i_1, i_2, \dots, i_N)$ to denote the (i_1, i_2, \dots, i_N) -th element of \mathcal{X} . For a third-order tensor

$\mathcal{X} \in \mathbb{R}^{I_1 \times I_2 \times I_3}$, we use $\mathbf{X}^{(n)} \in \mathbb{R}^{I_1 \times I_2}$ to denote the n -th frontal slice of \mathbf{X} . The symbol \odot denotes the Hadamard product (i.e., point-wise multiplication). The symbol \triangle denotes the face-wise product between two third-order tensors [18]. The rank of matrix \mathbf{X} is denoted as $\text{rank}(\mathbf{X})$. The Frobenius norm of tensor \mathcal{X} is defined as $\|\mathcal{X}\|_F = \sqrt{\sum_{i_1, i_2, \dots, i_N} |\mathcal{X}(i_1, i_2, \dots, i_N)|^2}$.

B. Preliminaries

Definition 1 (Generalized Unfolding [24]). *Given a permutation \mathbf{m} of the vector $(1, 2, \dots, N)$, the generalized unfolding of tensor $\mathcal{X} \in \mathbb{R}^{I_1 \times I_2 \times \dots \times I_N}$ corresponding to vector \mathbf{m} is defined as the matrix*

$$\mathbf{X}_{[\mathbf{m}(1:q); \mathbf{m}(q+1:N)]} = \text{reshape}^1 \left(\mathcal{X}^{\mathbf{m}}, \prod_{i=1}^q I_{\mathbf{m}(i)}, \prod_{i=q+1}^N I_{\mathbf{m}(i)} \right), \quad (1)$$

where $\mathcal{X}^{\mathbf{m}}$ is formed by permuting the modes of tensor \mathcal{X} according to the order of vector \mathbf{m} .

For example, the traditional mode- n unfolding of \mathcal{X} is $\mathbf{X}_{[n; 1, 2, \dots, n-1, n+1, \dots, N]}$, which is denoted by $\mathbf{X}_{\langle n \rangle}$.

1) *Factor Interaction*: Factor interaction serves as a key component of tensor decomposition, with different categories of it inducing distinct tensor decompositions. We will first introduce different factor interactions, including outer product, mode- n product, tensor contraction, and t-product.

Definition 2 (Outer Product [42]). *The outer product between vectors $\mathbf{a}_n \in \mathbb{R}^{I_n}$ ($n = 1, 2, \dots, N$) results in an N th-order tensor $\mathcal{X} \in \mathbb{R}^{I_1 \times I_2 \times \dots \times I_N}$, defined as*

$$\mathcal{X} = \mathbf{a}_1 \circ \mathbf{a}_2 \circ \dots \circ \mathbf{a}_N. \quad (2)$$

with elements as

$$\mathcal{X}(i_1, i_2, \dots, i_N) = \mathbf{a}_1(i_1) \mathbf{a}_2(i_2) \dots \mathbf{a}_N(i_N). \quad (3)$$

Definition 3 (Mode- n Product [42]). *The mode- n product between an N th-order tensor $\mathcal{X} \in \mathbb{R}^{I_1 \times I_2 \times \dots \times I_{n-1} \times I_n \times I_{n+1} \times \dots \times I_N}$ and a matrix $\mathbf{A} \in \mathbb{R}^{J \times I_n}$ results in an N th-order tensor $\mathcal{Y} \in \mathbb{R}^{I_1 \times I_2 \times \dots \times I_{n-1} \times J \times I_{n+1} \times \dots \times I_N}$, defined as*

$$\begin{aligned} & (\mathcal{X} \times_n \mathbf{A})(i_1, i_2, \dots, j, \dots, i_N) \\ &= \sum_{i_n=1}^{I_n} \mathcal{X}(i_1, i_2, \dots, i_n, \dots, i_N) \mathbf{A}(j, i_n). \end{aligned} \quad (4)$$

According to the above-mentioned two definitions, we have

$$\mathcal{Y} = \mathcal{X} \times_n \mathbf{A} \Leftrightarrow \mathbf{Y}_{\langle n \rangle} = \mathbf{A} \mathbf{X}_{\langle n \rangle}. \quad (5)$$

Definition 4 (Tensor Contraction [24]). *Let $\mathcal{A} \in \mathbb{R}^{J_1 \times J_2 \times \dots \times J_M}$ and $\mathcal{B} \in \mathbb{R}^{I_1 \times I_2 \times \dots \times I_N}$ share the same size in p modes (i.e., $J_{\mathbf{m}(q)} = I_{\mathbf{n}(q)}$ for $q = 1, 2, \dots, p$). The tensor contraction between \mathcal{A} and \mathcal{B} results in an $(M + N - 2p)$ th-order tensor \mathcal{X} , defined as $\mathcal{X} = \mathcal{A} \times_{\mathbf{m}(1:p)}^{\mathbf{n}(1:p)} \mathcal{B} \Leftrightarrow \mathbf{X}_{[1:M-p; M-p+1:M+N-2p]} = \mathbf{A}_{[\mathbf{m}(p+1:M); \mathbf{m}(1:p)]} \mathbf{B}_{[\mathbf{n}(1:p); \mathbf{n}(p+1:N)]}$.*

Definition 5 (T-Product [43]). *The invertible transform-based t-product between $\mathcal{A} \in \mathbb{R}^{I_1 \times I_2 \times I_3}$ and $\mathcal{B} \in \mathbb{R}^{I_2 \times I_4 \times I_3}$ is defined*

¹By following the notation of MATLAB commands.

as $\mathcal{A} *_M \mathcal{B} = ((\mathcal{A} \times_3 \mathbf{M}) \Delta (\mathcal{B} \times_3 \mathbf{M})) \times_3 \mathbf{M}^{-1} \in \mathbb{R}^{I_1 \times I_4 \times I_3}$, where $\mathbf{M} \in \mathbb{R}^{I_3 \times I_3}$ is the invertible matrix, and \mathbf{M}^{-1} is the inverse matrix of \mathbf{M} .

2) *Tensor Decomposition*: Based on the above factor interactions, different tensor decompositions are induced as follows.

Definition 6 (CP Decomposition [15]). For an N th-order tensor $\mathcal{X} \in \mathbb{R}^{I_1 \times I_2 \times \dots \times I_N}$, the CP decomposition is defined as

$$\mathcal{X} = \sum_{r=1}^R \mathbf{h}_r^1 \circ \mathbf{h}_r^2 \circ \dots \circ \mathbf{h}_r^N, \quad (6)$$

where $\mathbf{H}_n = [\mathbf{h}_1^n, \mathbf{h}_2^n, \dots, \mathbf{h}_R^n] \in \mathbb{R}^{I_n \times R}$ ($n = 1, 2, \dots, N$) is the factor matrix. The CP rank is defined as R .

Definition 7 (Tucker Decomposition [16]). For an N th-order tensor $\mathcal{X} \in \mathbb{R}^{I_1 \times I_2 \times \dots \times I_N}$, the Tucker decomposition is defined as

$$\mathcal{X} = \mathcal{C} \times_1 \mathbf{H}_1 \times_2 \mathbf{H}_2 \cdots \times_N \mathbf{H}_N, \quad (7)$$

where $\mathbf{H}_n \in \mathbb{R}^{I_n \times R_n}$ ($n = 1, 2, \dots, N$) is the factor matrix and $\mathcal{C} \in \mathbb{R}^{R_1 \times R_2 \times \dots \times R_N}$ is the N th-order core tensor. The Tucker rank is defined as the vector $[R_1, R_2, \dots, R_N]$.

Definition 8 (TT Decomposition [22], [44]). For an N th-order tensor $\mathcal{X} \in \mathbb{R}^{I_1 \times I_2 \times \dots \times I_N}$, the TT decomposition is defined as

$$\mathcal{X} = \mathbf{G}_1 \times_2^1 \mathcal{G}_2 \cdots \times_N^1 \mathbf{G}_N, \quad (8)$$

where $\mathcal{G}_n \in \mathbb{R}^{R_{n-1} \times I_n \times R_n}$ ($n = 2, \dots, N-1$) is the third-order factor tensor. $\mathbf{G}_1 \in \mathbb{R}^{I_1 \times R_1}$ and $\mathbf{G}_N \in \mathbb{R}^{R_{N-1} \times I_N}$ are the factor matrices. The TT rank is defined as the vector $[R_1, R_2, \dots, R_{N-1}]$.

Definition 9 (TR Decomposition [23], [44]). For an N th-order tensor $\mathcal{X} \in \mathbb{R}^{I_1 \times I_2 \times \dots \times I_N}$, the TR decomposition is defined as

$$\mathcal{X} = \mathcal{G}_1 \times_3^1 \mathcal{G}_2 \cdots \times_{n+1}^1 \mathcal{G}_n \cdots \times_{N+1,1}^{1,3} \mathcal{G}_N, \quad (9)$$

where $\mathcal{G}_n \in \mathbb{R}^{R_n \times I_n \times R_{n+1}}$ ($n = 1, 2, \dots, N; R_1 = R_{N+1}$) is the third-order factor tensor. The TR rank is defined as the vector $[R_1, R_2, \dots, R_N]$.

Definition 10 (FCTN Decomposition [24], [44]). For an N th-order tensor $\mathcal{X} \in \mathbb{R}^{I_1 \times I_2 \times \dots \times I_N}$, the FCTN decomposition is defined as

$$\mathcal{X} = \mathcal{G}_1 \times_{n_1}^{m_1^1} \mathcal{G}_2 \cdots \times_{n_{1:N-1}^{N-1}}^{m_{1:N-1}^{N-1}} \mathcal{G}_N, \quad (10)$$

where $\mathcal{G}_n \in \mathbb{R}^{R_{1,n} \times R_{2,n} \times \dots \times R_{n-1,n} \times I_n \times R_{n,n+1} \times \dots \times R_{n,N}}$ ($n = 1, 2, \dots, N$) is the N th-order factor tensor. The FCTN rank is defined as the vector collected by R_{n_1, n_2} ($1 \leq n_1 < n_2 \leq N$ and $n_1, n_2 \in \mathbb{N}^+$) and

$$\begin{cases} m_i^j = i, \\ n_i^j = 2 + (i-1)(N-j+1), \end{cases}$$

for $i = 1, 2, \dots, j$ and $j = 1, 2, \dots, N-1$.

Definition 11 (T-Product-Induced Tensor Factorization [45]). For a third-order tensor $\mathcal{X} \in \mathbb{R}^{I_1 \times I_2 \times I_3}$ with tubal-rank² up to R , the t -product-induced tensor factorization (TF) is defined as

$$\mathcal{X} = \mathcal{A} *_M \mathcal{B}, \quad (11)$$

where $\mathcal{A} \in \mathbb{R}^{I_1 \times R \times I_3}$ and $\mathcal{B} \in \mathbb{R}^{R \times I_2 \times I_3}$ are the third-order factor tensors. For efficiency, instead of adopting invertible matrix $\mathbf{M} \in \mathbb{R}^{I_3 \times I_3}$ and its inverse matrix \mathbf{M}^{-1} to obtain \mathcal{X} , we can cleverly start from the latent factor tensors $\hat{\mathcal{A}}_M \triangleq \mathcal{A} \times_3 \mathbf{M}$ and $\hat{\mathcal{B}}_M \triangleq \mathcal{B} \times_3 \mathbf{M}$ to reformulate the tensor factorization as

$$\mathcal{X} = (\hat{\mathcal{A}}_M \Delta \hat{\mathcal{B}}_M) \times_3 \mathbf{M}^{-1}. \quad (12)$$

Thus, we only need to learn factor tensors $\hat{\mathcal{A}}_M$ and $\hat{\mathcal{B}}_M$ to obtain \mathcal{X} , which avoids the complicated calculation of the $\mathcal{A} \times_3 \mathbf{M}$ and $\mathcal{B} \times_3 \mathbf{M}$ [12]. Furthermore, to enable flexible adaptation to different data, we can replace the invertible transform with a learnable linear transform, as formulated below:

$$\mathcal{X} = (\hat{\mathcal{A}} \Delta \hat{\mathcal{B}}) \times_3 \mathbf{L}, \quad (13)$$

where $\mathbf{L} \in \mathbb{R}^{\ell \times I_3}$ is a learnable linear transform, $\hat{\mathcal{A}} \in \mathbb{R}^{I_1 \times R \times \ell}$ and $\hat{\mathcal{B}} \in \mathbb{R}^{R \times I_2 \times \ell}$ are latent third-order factor tensors.

IV. TENSOR DECOMPOSITION STRUCTURE SEARCH FRAMEWORK

In this section, we elaborate on the design details of the proposed TenExp. Theoretically, we provide the approximation error bound of TenExp to reveal the approximation capability of TenExp. To examine the potential of the proposed TenExp, we evaluate it on the representative multi-dimensional data recovery task and suggest an unsupervised TenExp-based multi-dimensional data recovery model.

A. The Proposed TenExp

Selecting a suitable tensor decomposition to exactly capture the low-rank structures behind the data is at the heart of the tensor decomposition field, which remains a challenging and relatively under-explored problem. To address this problem, we elaborately design a mixture-of-experts-based tensor decomposition structure search framework. Due to the white box nature of tensor decomposition, TenExp can be trained in a fully unsupervised fashion solely from observational data, which can handle tensors of different orders and sizes, eliminating the need for any extra pre-constructed datasets. Specifically, we first systematically review tensor decompositions to provide a general cross-factor-interaction candidate search set. Based on the cross-factor-interaction candidate search set, we suggest a unified cross-factor-interaction energy-based rank estimation scheme for different tensor decompositions. To dynamically select and activate suitable tensor decompositions, we employ the top- k gating mechanism with learnable gating values, where only a selected subset of the cross-factor-interaction

²The tubal-rank of $\mathcal{X} \in \mathbb{R}^{I_1 \times I_2 \times I_3}$ is defined as $\text{rank}_t(\mathcal{X}) \triangleq \max_{n=1,2,\dots,I_3} \text{rank}((\mathcal{X} \times_3 \mathbf{M})^{(n)})$, where $\mathbf{M} \in \mathbb{R}^{I_3 \times I_3}$ is the invertible matrix.

candidate search set is activated. This framework enjoys two unique advantages over the state-of-the-art tensor decomposition structure search methods. Firstly, TenExp can provide a suitable single decomposition beyond a fixed factor-interaction family. Secondly, TenExp can deliver a suitable mixture of decompositions beyond a single decomposition.

In summary, the proposed TenExp is composed of three key components, i.e., the cross-factor-interaction candidate search set, the cross-factor-interaction energy-based rank estimation, and the gating mechanism; as shown in Fig. 1. The mathematical representation of TenExp can be expressed as follows:

$$\hat{\mathcal{X}} = \sum_{i=1}^L \lambda_{\theta_i} \mathcal{E}_{\phi_i}, \quad (14)$$

where $\hat{\mathcal{X}}$ is the data estimated by the proposed TenExp. $\{\mathcal{E}_{\phi_i}\}_{i=1}^L$ represent candidate tensor decompositions and $\{\phi_i\}_{i=1}^L$ denote the learnable parameters of candidate tensor decompositions. $\{\lambda_{\theta_i}\}_{i=1}^L$ are the normalized gating values and $\{\theta_i\}_{i=1}^L$ denote the learnable parameters of gating values. L denotes the number of candidate tensor decompositions. Now, we introduce the three components of the proposed TenExp.

1) *Cross-Factor-Interaction Candidate Search Set*: To offer a general candidate search set, we first conduct a systematic review of tensor decompositions. For tensor decomposition, the interaction between factors plays a crucial role. Hence, we reorganize the relationships between different tensor decompositions from a factor-interaction perspective and divide them into three categories: the mode- n product family (including CP and Tucker decompositions), the tensor contraction family (including TT, TR, and FCTN decompositions), and the t-product family (including TF).

Theorem 1. *Outer product-induced CP decomposition can be viewed as a special case of mode- n product-induced Tucker decomposition where the core tensor is superdiagonal and $R_1 = R_2 = \dots = R_N$ [42].*

Theorem 2. *Tensor contraction-induced TT decomposition can be viewed as a special case of tensor contraction-induced TR decomposition where the TR ranks $R_1 = 1$ [44].*

Theorem 3. *Tensor contraction-induced TT decomposition can be viewed as a special case of tensor contraction-induced FCTN decomposition where the FCTN ranks $R_{n_1, n_2} = 1(|n_1 - n_2| > 1)$ [44].*

Theorem 4. *For the third-order case, tensor contraction-induced TR decomposition is equivalent to tensor contraction-induced FCTN decomposition. For higher-order cases, tensor contraction-induced TR decomposition can be viewed as a special case of tensor contraction-induced FCTN decomposition where the FCTN ranks $R_{n_1, n_2} = 1(|n_1 - n_2| > 1)$ except for $R_{1, N}$ [44].*

Based on the above Theorems 1–4, we summarize the relationships of different factor-interaction families in the

third-order case as follows: (i) Tensor contraction-induced TT decomposition can be viewed as a special case of tensor contraction-induced FCTN decomposition. (ii) Outer product-induced CP decomposition can be viewed as a special case of mode- n product-induced Tucker decomposition. Therefore, for the third-order case, we consider Tucker decomposition, FCTN decomposition, and TF as the cross-factor-interaction candidate search set.

Similarly, the relationships between different factor-interaction families in the higher-order case can be summarized as follows: (i) Outer product-induced CP decomposition can be viewed as a special case of mode- n product-induced Tucker decomposition. (ii) Tensor contraction-induced TT decomposition can be viewed as a special case of tensor contraction-induced TR decomposition and FCTN decomposition. (iii) Tensor contraction-induced TR decomposition can be viewed as a special case of tensor contraction-induced FCTN decomposition. Notably, due to the standard t-product being only applicable to the third-order case. Therefore, for the higher-order case, we consider Tucker decomposition and FCTN decomposition as the cross-factor-interaction candidate search set.

Based on this rationally structured cross-factor-interaction candidate search set, we detail how to estimate ranks for different tensor decompositions in the following section.

2) *Cross-Factor-Interaction Energy-Based Rank Estimation*: Rank is a critical component of tensor decomposition, as it accurately characterizes the intrinsic structure of data. However, the definition of tensor rank varies substantially across distinct factor interactions, so it is important to find a unified cross-factor-interaction rank estimation scheme for different tensor decompositions. To achieve this goal, we proposed an energy-based scheme for rank estimation across all candidate tensor decompositions. Specifically, we define the accumulation energy ratio of top- k singular values as $\sum_{i=1}^k \sigma_i^2 / \sum_j \sigma_j^2$, where σ_i is i -th singular value. Then, we decompose the input matrix into “dominant components” (main information) and “secondary components” (redundancy information) and use the energy ratio threshold τ to determine the boundary between them. To exemplify this, the pseudocode for the energy-based rank estimation algorithm is provided in the algorithm 1.

3) *Gating Mechanism*: To dynamically select and activate suitable tensor decompositions, we employ the top- k gating mechanism with learnable gating values, where only a selected subset of the cross-factor-interaction candidate search set is activated. The softmax(\cdot) gating function models the probability distribution across candidate tensor decompositions by computing the weighted sum exclusively over the outputs of the top- k candidate tensor decompositions. The mathematical formulation of the top- k gating mechanism is presented as follows:

$$\lambda_{\theta_i} = \text{softmax}(\text{top}(\{g_{\theta_i}\}_{i=1}^L, k))_i, \quad (15)$$

where $\{\lambda_{\theta_i}\}_{i=1}^L$ are the normalized gating values, $\{g_{\theta_i}\}_{i=1}^L$ represent the gating values, $\{\theta_i\}_{i=1}^L$ denote the learnable parameters of gating values, and L denotes the number of candidate tensor decompositions. The $\text{top}(\cdot, k)$ function retains only the top- k entries of a vector at their original values, while setting all other entries to $-\infty$. Following the softmax(\cdot)

operation, those entries assigned $-\infty$ become approximately zero.

Based on this gating mechanism, the proposed TenExp not only can provide a suitable single decomposition but also can deliver a suitable mixture of decompositions, which is detailed below.

Remark 1. *The search results of the proposed TenExp with different top-k values:*

- When $k = 1$, the proposed TenExp provides a suitable single decomposition.
- When $k > 1$, the proposed TenExp delivers a suitable mixture of decompositions.

Current tensor decomposition structure search methods are still confined by a fixed factor-interaction family (e.g., tensor contraction) and cannot deliver the mixture of decompositions.

Remark 2. *The complexity analysis of the proposed TenExp with different top-k values:*

- When $k < L$, the proposed TenExp activates top-k candidate tensor decompositions, making effective parameters lower than total.
- When $k = L$, even if all candidate tensor decompositions are activated, the low-rank structure design can alleviate parameter explosion.

B. The Approximation Error Bound of TenExp

Theoretically, we provide the approximation error bound of TenExp in theorem 5, which reveals the approximation capability of TenExp, clarifying its capability to approximate arbitrary tensors within a guaranteed error range; see Fig. 2 for the comparison between candidate tensor decompositions and the proposed TenExp.

Theorem 5 (Approximation Error Bound of TenExp). *Let $\mathcal{X} \in \mathbb{R}^{I_1 \times I_2 \times I_3}$ be a third-order³ tensor with Tucker rank $[R_1, R_2, R_3]$, FCTN rank $[R_{1,2}, R_{1,3}, R_{2,3}]$, TF tubal-rank R and latent dimension ℓ . Consider the TenExp representation:*

$$\hat{\mathcal{X}} = \sum_{i=1}^3 \lambda_{\theta_i} \mathcal{E}_{\phi_i},$$

where $\{\mathcal{E}_{\phi_i}\}_{i=1}^3 \in \mathbb{R}^{I_1 \times I_2 \times I_3}$ represent the candidate Tucker decomposition, FCTN decomposition, and TF, respectively. $\{\lambda_{\theta_i}\}_{i=1}^3$ are the normalized gating values. Under the following assumptions:

- $\|\mathcal{X}\|_F \leq K$, K is a constant.
- The factor matrices \mathbf{H}_n of Tucker decomposition are orthogonal.
- The linear transform matrix \mathbf{L} of TF is semi-orthogonal.
- $R_n \leq \text{rank}(\mathbf{X}_{\langle n \rangle}) \forall n \in \{1, 2, 3\}$.
- $R_{n_1, n_2} \leq \min(\text{rank}(\mathbf{X}_{\langle n_1 \rangle}, \mathbf{X}_{\langle n_2 \rangle})) \forall n_1, n_2 \in \{1, 2, 3\}$ and $n_1 < n_2$.
- $R \leq \text{rank}(\mathbf{X}^{(n)}) \forall n \in \{1, 2, \dots, \ell\}$.
- $\ell \leq \text{rank}(\mathbf{X}_{\langle 3 \rangle})$.

³This approximation error bound of TenExp can be easily extended to higher-order.

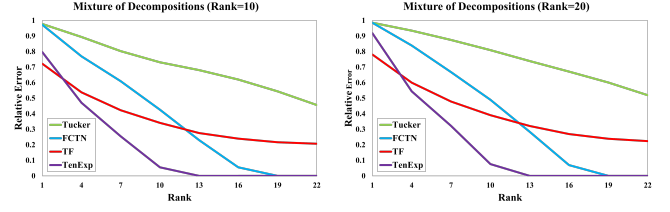


Fig. 2: Comparison between candidate tensor decompositions and our proposed TenExp in terms of relative error for fitting synthetic data. “Mixture of Decompositions” denotes a uniform mixture strategy for Tucker decomposition, FCTN decomposition, and TF. For simplicity, we uniformly set all ranks of Tucker decomposition, FCTN decomposition, and TF as the same values.

the approximation error bound of TenExp satisfies:

$$\begin{aligned} & \|\mathcal{X} - \hat{\mathcal{X}}\|_F^2 \\ & \leq \lambda_{\theta_1}^2 \sum_{n=1}^3 \sum_{i=R_n+1}^{\text{rank}(\mathbf{X}_{\langle n \rangle})} \sigma_i^2(\mathbf{X}_{\langle n \rangle}) \\ & + \lambda_{\theta_2}^2 \sum_{n_1=1}^2 \sum_{n_2=n_1+1}^3 \sum_{i=R_{n_1, n_2}+1}^{\text{rank}(\mathbf{X}_{\langle n_1 n_2 \rangle})} \sigma_i^2(\mathbf{X}_{\langle n_1 n_2 \rangle}) \\ & + \lambda_{\theta_3}^2 \left(\sum_{n=1}^{\ell} \sum_{i=R+1}^{\text{rank}(\mathbf{X}^{(n)})} \sigma_i^2(\mathbf{X}^{(n)}) + \sum_{i=\ell+1}^{\text{rank}(\mathbf{X}_{\langle 3 \rangle})} \sigma_i^2(\mathbf{X}_{\langle 3 \rangle}) \right), \end{aligned} \quad (16)$$

where $\sigma_i(\cdot)$ denotes the i -th singular value and $\mathbf{X}_{\langle n_1 n_2 \rangle}$ represents the matrix with the smaller rank between $\mathbf{X}_{\langle n_1 \rangle}$ and $\mathbf{X}_{\langle n_2 \rangle}$.

Proof. Based on the TenExp representation, a third-order tensor $\mathcal{X} \in \mathbb{R}^{I_1 \times I_2 \times I_3}$ can be estimated by $\hat{\mathcal{X}} = \sum_{i=1}^3 \lambda_{\theta_i} \mathcal{E}_{\phi_i}$. Substituting the TenExp representation into $\|\mathcal{X} - \hat{\mathcal{X}}\|_F^2$, the error bound of approximation can be formulated as

$$\begin{aligned} \|\mathcal{X} - \hat{\mathcal{X}}\|_F^2 & = \|\mathcal{X} - \sum_{i=1}^3 \lambda_{\theta_i} \mathcal{E}_{\phi_i}\|_F^2 \\ & = \left\| \sum_{i=1}^3 \lambda_{\theta_i} (\mathcal{X} - \mathcal{E}_{\phi_i}) \right\|_F^2 \\ & \leq \sum_{i=1}^3 \lambda_{\theta_i} \|\mathcal{X} - \mathcal{E}_{\phi_i}\|_F^2. \end{aligned} \quad (17)$$

Thus, the approximation error bound of TenExp reduces to the combination of the approximation error bound corresponding to each individual decomposition. The approximation error bound of each decomposition is given as follows:

- $\|\mathcal{X} - \mathcal{E}_{\phi_1}\|_F^2 \leq \sum_{n=1}^3 \sum_{i=R_n+1}^{\text{rank}(\mathbf{X}_{\langle n \rangle})} \sigma_i^2(\mathbf{X}_{\langle n \rangle})$.
- $\|\mathcal{X} - \mathcal{E}_{\phi_2}\|_F^2 \leq \sum_{n_1=1}^2 \sum_{n_2=n_1+1}^3 \sum_{i=R_{n_1, n_2}+1}^{\text{rank}(\mathbf{X}_{\langle n_1 n_2 \rangle})} \sigma_i^2(\mathbf{X}_{\langle n_1 n_2 \rangle})$.
- $\|\mathcal{X} - \mathcal{E}_{\phi_3}\|_F^2 \leq \sum_{n=1}^{\ell} \sum_{i=R+1}^{\text{rank}(\mathbf{X}^{(n)})} \sigma_i^2(\mathbf{X}^{(n)}) + \sum_{i=\ell+1}^{\text{rank}(\mathbf{X}_{\langle 3 \rangle})} \sigma_i^2(\mathbf{X}_{\langle 3 \rangle})$.

Combining these steps, we can obtain Eq.(16).

Algorithm 1 Cross-Factor-Interaction Energy-Based Rank Estimation

Input: An N th-order ($N \geq 3$) tensor $\mathcal{X} \in \mathbb{R}^{I_1 \times I_2 \times \dots \times I_N}$ and the energy ratio thresholds $\{\tau_i\}_{i=1}^3$.

Output: Estimated rank and parameter corresponding to the specified decomposition type.

- 1: **Energy-Based Rank Estimation** ERM(\mathbf{X}, τ);
 - 2: Compute SVD of input matrix \mathbf{X} : $\sigma_1 \geq \sigma_2 \geq \dots \geq \sigma_n \geq 0$ (singular values) and left singular matrix \mathbf{U} ;
 - 3: **Initialization:** $E_{\text{total}} = \sum_{j=1}^n \sigma_j^2$, $E_{\text{accum}} = 0$, estimated rank $\hat{r} = 0$;
 - 4: **for** $k = 1$ to n **do**
 - 5: Compute $E_{\text{accum}} += \sigma_k^2$; $E_{\text{ratio}} = E_{\text{accum}}/E_{\text{total}}$;
 - 6: **if** $E_{\text{ratio}} \geq \tau$ **then**
 - 7: $\hat{r} = k$ and break.
 - 8: **end if**
 - 9: **end for**
 - 10: **return** Estimated rank \hat{r} and truncated left singular matrix $\mathbf{U}(:, 1 : \hat{r})$.
 - 11: **if** Rank Estimation for Tucker **then**
 - 12: **for** $n = 1$ to N **do**
 - 13: Estimated rank($\mathbf{X}_{\langle n \rangle}$) by ERM($\mathbf{X}_{\langle n \rangle}, \tau_1$);
 - 14: **end for**
 - 15: Compute Tucker rank $R_n = \text{rank}(\mathbf{X}_{\langle n \rangle})$.
 - 16: **else if** Rank Estimation for FCTN **then**
 - 17: **for** $n = 1$ to N **do**
 - 18: Estimate rank($\mathbf{X}_{\langle n \rangle}$) by ERM($\mathbf{X}_{\langle n \rangle}, \tau_2$);
 - 19: **end for**
 - 20: Compute FCTN rank $R_{n_1, n_2} = \min(\text{rank}(\mathbf{X}_{\langle n_1 \rangle}), \text{rank}(\mathbf{X}_{\langle n_2 \rangle}))$.
 - 21: **else if** Rank Estimation for TF **then**
 - 22: Estimate rank($\mathbf{X}_{\langle 3 \rangle}$) and truncated left singular matrix $\hat{\mathbf{L}}$ by ERM($\mathbf{X}_{\langle 3 \rangle}, \tau_3$);
 - 23: **for** $n = 1$ to $\text{rank}(\mathbf{X}_{\langle 3 \rangle})$ **do**
 - 24: Estimate rank($(\mathcal{X} \times_3 \hat{\mathbf{L}}^\top)^{(n)}$) by ERM($(\mathcal{X} \times_3 \hat{\mathbf{L}}^\top)^{(n)}, \tau_3$);
 - 25: **end for**
 - 26: Compute TF tubal-rank $R = \max_{n=1,2,\dots,\text{rank}(\mathbf{X}_{\langle 3 \rangle})} \text{rank}((\mathcal{X} \times_3 \hat{\mathbf{L}}^\top)^{(n)})$.
 - 27: Compute latent dimension $\ell = \text{rank}(\mathbf{X}_{\langle 3 \rangle})$.
 - 28: **end if**
-

C. Unsupervised Multi-Dimensional Data Recovery Model

To examine the potential of the proposed TenExp, we evaluate it on the representative multi-dimensional data recovery task and suggest an unsupervised TenExp-based multi-dimensional data recovery model as follows:

$$\begin{aligned}
 & \min_{\{\phi_i\}_{i=1}^L, \{\theta_i\}_{i=1}^L} \|\mathcal{M} \odot (\hat{\mathcal{X}} - \mathcal{O})\|_F^2, \\
 & \text{s.t. } \hat{\mathcal{X}} = \sum_{i=1}^k \lambda_{\theta_i} \mathcal{E}_{\phi_i}, \\
 & \lambda_{\theta_i} = \text{softmax}(\text{top}(\{g_{\theta_i}\}_{i=1}^L, k))_i,
 \end{aligned} \tag{18}$$

where \mathcal{O} is the observed multi-dimensional data and $\hat{\mathcal{X}}$ is the data estimated by the proposed TenExp. \mathcal{M} is a binary mask

Algorithm 2 Unsupervised Multi-Dimensional Data Recovery Model

Input: Observed data \mathcal{O} , observed binary mask \mathcal{M} , energy ratio thresholds $\{\tau_i\}_{i=1}^L$, number of max iterations t_{max} , and top- k value.

Output: Recovered data \mathcal{X} .

- 1: **Initialization:** Candidate tensor decompositions $\{\mathcal{E}_{\phi_i}\}_{i=1}^L$ and gating values $\{g_{\theta_i}\}_{i=1}^L$;
 - 2: Estimate ranks for candidate tensor decompositions via algorithm1;
 - 3: **for** $t = 1$ to t_{max} **do**
 - 4: Compute estimated data $\hat{\mathcal{X}} = \sum_{i=1}^L \lambda_{\theta_i} \mathcal{E}_{\phi_i}$ with top- L ;
 - 5: Alternating update $\{\phi_i\}_{i=1}^L$ and $\{\theta_i\}_{i=1}^L$ via Adam;
 - 6: **end for**
 - 7: **if** $k < L$ **then**
 - 8: **Reinitialization:** The selected candidate tensor decompositions $\{\mathcal{E}_{\theta_i}\}_{i=1}^k$;
 - 9: **for** $t = 1$ to t_{max} **do**
 - 10: Compute estimated data $\hat{\mathcal{X}} = \sum_{i=1}^k \lambda_{\theta_i} \mathcal{E}_{\phi_i}$ with top- k ;
 - 11: Update $\{\phi_i\}_{i=1}^k$ via Adam;
 - 12: **end for**
 - 13: **end if**
 - 14: **if** $\mathcal{M} == 1$ **then**
 - 15: Compute recovered data $\mathcal{X} = \hat{\mathcal{X}}$.
 - 16: **else if** $\mathcal{M} \neq 1$ **then**
 - 17: Compute recovered data $\mathcal{X} = \mathcal{M} \odot \hat{\mathcal{X}} + (1 - \mathcal{M}) \odot \mathcal{O}$.
 - 18: **end if**
-

tensor that sets the observed location to ones and others to zeros. Specifically, when \mathcal{M} is an all-ones tensor, this recovery model degenerates to a data fitting model. When \mathcal{M} is not an all-ones tensor, this recovery model is a data completion model. $\{\mathcal{E}_{\phi_i}\}_{i=1}^L$ are the candidate tensor decompositions and $\{\phi_i\}_{i=1}^L$ denote the learnable parameters of candidate tensor decompositions. $\{\lambda_{\theta_i}\}_{i=1}^k$ are the normalized gating values, $\{g_{\theta_i}\}_{i=1}^L$ are the gating values, and $\{\theta_i\}_{i=1}^L$ denote the learnable parameters of gating values. L denotes the number of candidate tensor decompositions. The $\text{top}(\cdot, k)$ function retains only the top- k entries of a vector at their original values, while setting all other entries to $-\infty$.

To solve model (18), we leverage the adaptive moment estimation (Adam) algorithm [46], which is widely used in deep learning, to efficiently optimize the parameter set $\psi = \{\{\phi_i\}_{i=1}^L, \{\theta_i\}_{i=1}^L\}$. We summarize the complete procedure of the proposed unsupervised TenExp-based multi-dimensional data recovery model in algorithm 2.

V. EXPERIMENTS

To verify the effectiveness and superiority of the proposed TenExp, we conduct extensive comparative experiments and analyses on various multi-dimensional datasets, encompassing both synthetic and realistic datasets (including MSIs, color videos, and light field data). First, we provide a detailed introduction to the experimental settings, followed by the corresponding experimental results and in-depth analysis. All experiments are performed on a PC equipped with one Intel(R)

TABLE II: Quantitative comparison of CR (\downarrow) and RE (\downarrow) of different methods on third-order synthetic data.

Method	Rank: 3		Rank: 5		Rank: 7	
	CR	RE	CR	RE	CR	RE
Synthetic Data (Tucker)						
Tucker	0.3%	$3 * 10^{-5}$	0.7%	$2 * 10^{-5}$	1.1%	$2 * 10^{-5}$
TF	0.4%	$4 * 10^{-1}$	1.0%	$2 * 10^{-1}$	1.9%	$2 * 10^{-1}$
TNGreedy	0.4%	$6 * 10^{-2}$	1.5%	$9 * 10^{-4}$	3.0%	$8 * 10^{-4}$
SVDinsTN	0.6%	$8 * 10^{-4}$	2.2%	$5 * 10^{-4}$	4.3%	$2 * 10^{-4}$
TenExp	0.3%	$3 * 10^{-5}$	0.7%	$2 * 10^{-5}$	1.1%	$2 * 10^{-5}$
Synthetic Data (FCTN)						
Tucker	1.0%	$4 * 10^{-1}$	3.4%	$6 * 10^{-1}$	8.0%	$6 * 10^{-1}$
TF	1.4%	$4 * 10^{-1}$	3.6%	$6 * 10^{-1}$	6.8%	$7 * 10^{-1}$
TNGreedy	1.0%	$5 * 10^{-4}$	3.4%	$5 * 10^{-5}$	5.8%	$8 * 10^{-4}$
SVDinsTN	1.6%	$2 * 10^{-4}$	5.2%	$9 * 10^{-4}$	8.9%	$1 * 10^{-3}$
TenExp	1.0%	$1 * 10^{-5}$	3.0%	$1 * 10^{-5}$	5.8%	$9 * 10^{-5}$
Synthetic Data (TF)						
Tucker	6.9%	$2 * 10^{-1}$	8.2%	$3 * 10^{-1}$	9.2%	$4 * 10^{-1}$
TF	6.0%	$2 * 10^{-5}$	7.6%	$2 * 10^{-5}$	8.4%	$2 * 10^{-5}$
TNGreedy	6.4%	$7 * 10^{-1}$	7.6%	$8 * 10^{-1}$	9.0%	$8 * 10^{-1}$
SVDinsTN	6.8%	$8 * 10^{-1}$	8.3%	$8 * 10^{-1}$	10.7%	$7 * 10^{-1}$
TenExp	6.0%	$2 * 10^{-5}$	7.6%	$2 * 10^{-5}$	8.4%	$2 * 10^{-5}$
Synthetic Data (Mixture of Decompositions)						
Tucker	30.7%	$3 * 10^{-2}$	59.1%	$1 * 10^{-1}$	86.8%	$1 * 10^{-1}$
TF	29.1%	$4 * 10^{-1}$	56.2%	$4 * 10^{-1}$	89.6%	$4 * 10^{-1}$
TNGreedy	29.3%	$6 * 10^{-2}$	54.3%	$2 * 10^{-2}$	87.3%	$8 * 10^{-3}$
SVDinsTN	43.2%	$9 * 10^{-2}$	67.0%	$5 * 10^{-2}$	89.5%	$4 * 10^{-2}$
TenExp	28.7%	$1 * 10^{-4}$	54.0%	$1 * 10^{-4}$	85.5%	$1 * 10^{-4}$

Core(TM) i7-8700K CPU, one NVIDIA GeForce RTX 4070 Ti GPU, and 32 GB RAM. The proposed TenExp are implemented by using Python and the PyTorch library with GPU calculation.

A. Fitting Experiments for Synthetic and Realistic Datasets

1) *Evaluation Metrics*: To quantitatively evaluate the performance of different methods, we adopted two widely used metrics: the compression rate (CR) and the relative error (RE). CR is defined as $N_S/N_{\mathcal{X}} \times 100\%$, with N_S denoting the number of elements in the factor matrices/tensors, and $N_{\mathcal{X}}$ representing the total number of elements in the original tensor. RE is defined as $\|\mathcal{X} - \hat{\mathcal{X}}\|_F / \|\mathcal{X}\|_F$, where \mathcal{X} is the original tensor and $\hat{\mathcal{X}}$ is the estimated tensor.

2) *Compared Methods*: To comprehensively evaluate the effectiveness of TenExp for synthetic data, we compare it against four classic tensor decomposition structure search methods: Tucker [16], TF [45], TNGreedy [34], and SVDinsTN [41]. For the sake of fairness, the rank settings of Tucker and TF are also estimated by algorithm 1.

3) *Experimental Data*: For synthetic data of size $50 \times 50 \times 50$, we first randomly generate the factor matrices/tensors of Tucker decomposition, FCTN decomposition, and TF, where all elements of these factors follow a Gaussian distribution (with values constrained between 0 and 1). Then, the synthetic tensors are constructed via the specific factor interactions detailed in Section III. For realistic data, we collect three MSIs² (*Cloth*, *Beads*, and *Jelly*) as testing data.

²Available at <https://cave.cs.columbia.edu/repository/Multispectral>

TABLE III: Quantitative comparison of CR (\downarrow) and RE (\downarrow) of different methods on realistic MSIs.

Method	<i>Cloth</i>		<i>Beads</i>		<i>Jelly</i>	
	CR	RE	CR	RE	CR	RE
Tucker	37.8%	$1 * 10^{-2}$	39.3%	$1 * 10^{-2}$	34.5%	$1 * 10^{-2}$
TF	34.4%	$1 * 10^{-2}$	39.0%	$1 * 10^{-2}$	35.4%	$1 * 10^{-2}$
TNGreedy	31.7%	$7 * 10^{-3}$	37.8%	$6 * 10^{-3}$	32.9%	$7 * 10^{-3}$
SVDinsTN	32.8%	$7 * 10^{-3}$	39.9%	$9 * 10^{-3}$	34.8%	$8 * 10^{-3}$
TenExp	31.7%	$6 * 10^{-3}$	37.8%	$5 * 10^{-3}$	32.6%	$6 * 10^{-3}$

4) Experimental Results of Synthetic and Realistic Data:

To systematically evaluate the performance of the proposed TenExp, we conduct fitting experiments on synthetic third-order tensor datasets and realistic MSIs. Tables II and III summarize the full quantitative results of the compared methods and the proposed TenExp.

In Table II, several experimental settings and notation definitions need to be clarified to avoid confusion: (i) The column labeled ‘‘Rank’’ refers to the ranks used for Tucker decomposition, FCTN decomposition, and TF. For simplicity, we uniformly set all ranks of Tucker decomposition, FCTN decomposition, and TF as the same values. Meanwhile, we set the latent dimension ℓ of TF as 10. (ii) The terms ‘‘Tucker’’, ‘‘FCTN’’, and ‘‘TF’’ in the table denote synthetic single decompositions. These data are designed to verify the effectiveness of top-1 TenExp. (iii) The term ‘‘Mixture of Decompositions’’ in the table denotes a uniform mixture strategy for candidate tensor decompositions. This strategy involves combining all candidate tensor decompositions at equal weights to verify the effectiveness of top- L TenExp. In Table III, to evaluate the effectiveness of TenExp for complex realistic data, we compare top- L TenExp against other tensor decomposition structure search methods.

The results in Tables II-III reveal two interesting findings: First, for single decomposition, the proposed TenExp can dynamically provide a suitable single decomposition beyond a fixed factor-interaction family. This advantage is reflected in smaller or the same relative errors with almost the same CR compared to competitors, which can only search single decompositions with a fixed factor-interaction family. Second, for mixture of decompositions and realistic MSIs, TenExp achieves significantly better results than classic tensor decomposition structure search methods, which can be attributed to delivering a suitable mixture of decompositions beyond a single decomposition.

B. Completion Experiments for Realistic Datasets

1) *Evaluation Metrics*: To quantitatively evaluate the performance of different methods, we adopted three widely used evaluation metrics: peak signal-to-noise ratio (PSNR), structural similarity index measure (SSIM), and RE. In general, higher PSNR and SSIM values, and lower RE values, indicate better performance of the evaluated methods.

2) *Compared Methods*: To comprehensively evaluate the effectiveness of TenExp for complex realistic data, we compare top- L TenExp against six classical tensor decomposition-based methods: HaLRTC [47], SiLRTCTT [26], TRLRF [48],

TABLE IV: The quantitative results for realistic MSI completion by different methods. The **best** and second-best values are highlighted.

SR		0.1			0.15			0.2			0.25			0.3		
Data	Method	PSNR	SSIM	RE												
<i>Flowers</i> (256×256×31)	HaLRTC	20.54	0.672	0.592	29.89	0.830	0.202	31.73	0.864	0.163	33.50	0.888	0.133	33.86	0.895	0.127
	SiLRCTCT	28.06	0.749	0.249	31.22	0.809	0.173	33.53	0.843	0.132	35.44	0.864	0.106	36.93	0.880	0.089
	TRLRF	20.32	0.552	0.607	25.34	0.568	0.340	26.52	0.656	0.297	26.81	0.670	0.287	27.09	0.685	0.278
	HTNN	29.94	0.790	0.200	32.92	0.844	0.142	34.70	0.873	0.116	36.28	0.890	0.096	37.41	0.894	0.085
	LTNN	29.74	0.784	0.205	32.95	0.840	0.142	34.81	0.869	0.114	36.32	0.886	0.096	37.52	0.898	0.083
	SVDinsTN	<u>35.03</u>	<u>0.887</u>	<u>0.111</u>	<u>37.28</u>	<u>0.890</u>	<u>0.086</u>	<u>38.18</u>	<u>0.901</u>	<u>0.077</u>	<u>40.22</u>	<u>0.930</u>	<u>0.061</u>	<u>41.63</u>	<u>0.940</u>	<u>0.052</u>
	TenExp	37.86	0.894	0.080	40.78	0.936	0.057	42.70	0.939	0.046	44.35	0.942	0.038	45.64	0.955	0.032
<i>Beers</i> (256×256×31)	HaLRTC	33.03	0.952	0.065	36.10	0.972	0.045	38.69	0.982	0.034	40.77	0.988	0.026	42.42	0.991	0.022
	SiLRCTCT	31.22	0.925	0.080	34.00	0.952	0.058	36.29	0.967	0.045	38.07	0.975	0.036	39.61	0.981	0.030
	TRLRF	34.83	0.945	0.053	36.69	0.960	0.042	38.19	0.969	0.036	39.56	0.976	0.030	41.10	0.982	0.025
	HTNN	32.36	0.928	0.070	39.73	0.983	0.030	42.32	0.990	0.022	44.45	0.993	0.017	46.08	0.995	0.014
	LTNN	33.53	0.934	0.061	38.29	0.977	0.035	41.34	0.987	0.025	43.84	0.993	0.018	45.89	0.995	0.014
	SVDinsTN	<u>37.99</u>	<u>0.973</u>	<u>0.036</u>	<u>40.60</u>	<u>0.983</u>	<u>0.027</u>	<u>42.72</u>	<u>0.988</u>	<u>0.021</u>	43.88	0.990	0.018	45.28	0.992	0.015
	TenExp	43.17	0.991	0.020	46.28	0.995	0.014	48.79	0.997	0.010	49.91	0.998	0.009	50.54	0.998	0.008
<i>Balloons</i> (256×256×31)	HaLRTC	31.64	0.932	0.120	34.91	0.959	0.082	37.55	0.975	0.061	39.60	0.983	0.048	41.61	0.988	0.038
	SiLRCTCT	30.75	0.910	0.133	33.81	0.941	0.093	36.01	0.958	0.072	37.89	0.968	0.058	39.53	0.976	0.048
	TRLRF	34.03	0.919	0.091	35.89	0.936	0.073	37.93	0.959	0.058	39.16	0.967	0.050	40.37	0.974	0.044
	HTNN	34.91	0.943	0.082	38.75	0.973	0.053	41.19	0.984	0.040	43.21	0.990	0.031	45.19	0.993	0.025
	LTNN	34.22	0.931	0.089	38.15	0.970	0.057	40.71	0.983	0.042	43.02	0.990	0.032	45.19	0.993	0.025
	SVDinsTN	<u>37.55</u>	<u>0.964</u>	<u>0.061</u>	<u>40.18</u>	<u>0.978</u>	<u>0.045</u>	<u>42.08</u>	<u>0.985</u>	<u>0.036</u>	43.61	0.988	0.030	45.10	0.991	0.025
	TenExp	44.46	0.991	0.027	48.23	0.996	0.017	49.49	0.996	0.015	51.48	0.997	0.012	52.76	0.998	0.010
<i>Feathers</i> (256×256×31)	HaLRTC	20.49	0.695	0.450	27.74	0.862	0.195	29.61	0.896	0.157	31.31	0.920	0.129	32.91	0.938	0.107
	SiLRCTCT	28.78	0.858	0.173	32.14	0.910	0.117	34.49	0.938	0.089	36.40	0.954	0.072	38.01	0.965	0.059
	TRLRF	31.28	0.837	0.130	33.43	0.889	0.101	35.19	0.922	0.082	36.35	0.938	0.072	36.99	0.943	0.067
	HTNN	28.28	0.830	0.183	32.58	0.910	0.111	34.70	0.940	0.087	36.36	0.957	0.072	37.83	0.969	0.061
	LTNN	29.08	0.837	0.167	32.74	0.912	0.109	34.79	0.943	0.086	36.41	0.959	0.072	37.88	0.970	0.060
	SVDinsTN	<u>34.46</u>	<u>0.936</u>	<u>0.090</u>	<u>37.23</u>	<u>0.961</u>	<u>0.065</u>	<u>38.83</u>	<u>0.971</u>	<u>0.054</u>	40.17	0.976	0.046	41.18	0.980	0.041
	TenExp	37.19	0.956	0.065	39.42	0.974	0.050	42.54	0.984	0.035	43.86	0.988	0.030	46.63	0.992	0.022

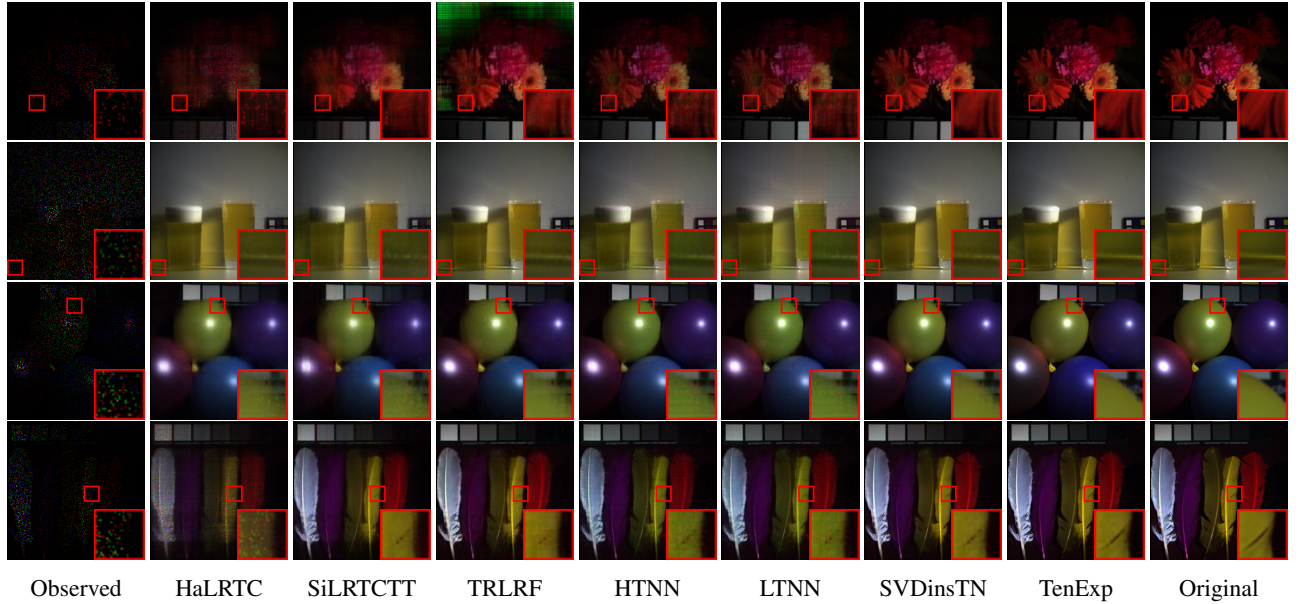


Fig. 3: The completion results of MSIs by different methods on *Flowers*, *Beers*, *Balloons*, and *Feathers* with SR = 0.1.

HTNN [49], LTNN [50], and SVDinsTN [41]. To ensure all methods operate at their peak performance, their respective hyperparameters are carefully tuned.

3) *Experimental Data*: We collect four MSIs (*Flowers*, *Beers*, *Balloons*, and *Feathers*), four color videos³ (*News*, *Claire*, *Grandma*, and *Akiyo*), and four light field data⁴ (*Greek*,

Museum, *Medieval2*, and *Vinyl*) as testing data. The sampling rates (SRs) are set as [0.1, 0.15, 0.2, 0.25, 0.3]. Before the experiments, the gray values of all datasets are normalized into the interval [0, 1].

4) *Experimental Results of Multispectral Images*: Table IV reports the PSNR, SSIM, and RE values for the completion results of different tensor decomposition-based methods on MSIs. Among these methods, HTNN and SVDinsTN

³Available at <https://traces.cnets.io/trace.eas.asu.edu/yuv/index.html>

⁴Available at <http://hci-lightfield.iwr.uni-heidelberg.de>

TABLE V: The quantitative results for realistic color video completion by different methods. The **best** and **second-best** values are highlighted.

SR		0.1			0.15			0.2			0.25			0.3		
Data	Method	PSNR	SSIM	RE												
<i>News</i> (144×176×3×30)	HaLRTC	18.24	0.589	0.328	22.09	0.705	0.211	24.28	0.772	0.164	25.72	0.814	0.138	27.08	0.848	0.118
	SiLRTCTT	27.18	0.851	0.117	29.84	0.903	0.086	31.81	0.931	0.068	33.36	0.947	0.057	34.67	0.959	0.049
	TRLRF	29.75	0.861	0.087	30.11	0.863	0.083	31.02	0.882	0.075	33.10	0.919	0.059	34.82	0.942	0.048
	HTNN	31.70	<u>0.916</u>	<u>0.069</u>	<u>33.53</u>	<u>0.939</u>	<u>0.056</u>	<u>34.94</u>	<u>0.953</u>	<u>0.048</u>	<u>36.13</u>	0.962	<u>0.041</u>	<u>37.35</u>	<u>0.970</u>	<u>0.036</u>
	LTNN	27.24	0.860	0.116	31.29	0.929	0.073	33.54	0.952	0.056	35.13	<u>0.964</u>	0.047	36.58	0.972	0.039
	SVDinsTN	31.58	0.897	0.070	33.16	0.922	0.058	<u>34.95</u>	0.945	<u>0.048</u>	36.07	0.958	0.042	37.16	0.967	0.037
	TenExp	33.13	0.924	0.059	34.98	0.946	0.047	36.60	0.960	0.039	37.47	0.965	0.035	38.60	0.972	0.031
<i>Claire</i> (144×176×3×30)	HaLRTC	19.86	0.632	0.214	27.00	0.859	0.094	29.58	0.897	0.070	31.11	0.918	0.058	32.60	0.935	0.049
	SiLRTCTT	29.74	0.884	0.068	32.42	0.921	0.050	34.34	0.941	0.040	35.87	0.954	0.034	37.21	0.962	0.029
	TRLRF	33.67	0.922	0.043	35.08	0.935	0.037	36.06	0.945	0.033	38.05	0.963	0.026	38.42	0.964	0.025
	HTNN	34.42	0.940	0.040	36.33	0.955	0.032	37.81	0.965	0.027	39.23	0.973	0.023	40.54	0.978	0.019
	LTNN	32.13	0.922	0.052	35.31	0.952	0.036	37.27	0.963	0.028	39.21	0.974	0.023	40.91	0.980	0.019
	SVDinsTN	<u>34.73</u>	0.933	<u>0.038</u>	<u>37.12</u>	<u>0.956</u>	<u>0.029</u>	<u>38.29</u>	0.964	<u>0.025</u>	<u>40.64</u>	<u>0.975</u>	<u>0.019</u>	<u>41.65</u>	<u>0.979</u>	<u>0.017</u>
	TenExp	36.19	0.947	0.032	38.00	0.961	0.026	39.20	0.967	0.023	41.15	0.976	0.018	42.00	0.978	0.016
<i>Grandma</i> (144×176×3×30)	HaLRTC	23.82	0.705	0.236	27.22	0.793	0.159	29.04	0.838	0.129	30.62	0.872	0.107	32.13	0.899	0.090
	SiLRTCTT	30.57	0.885	0.108	33.52	0.926	0.077	35.52	0.946	0.061	37.08	0.958	0.051	38.39	0.965	0.044
	TRLRF	32.88	0.879	0.083	34.46	0.908	0.069	36.44	0.937	0.055	37.83	0.953	0.047	38.26	0.956	0.044
	HTNN	<u>36.65</u>	<u>0.946</u>	<u>0.053</u>	<u>38.16</u>	<u>0.959</u>	<u>0.045</u>	<u>39.35</u>	<u>0.967</u>	<u>0.039</u>	<u>40.31</u>	<u>0.973</u>	<u>0.035</u>	<u>41.34</u>	<u>0.977</u>	<u>0.031</u>
	LTNN	33.40	0.928	0.078	37.96	<u>0.963</u>	0.046	<u>39.70</u>	<u>0.971</u>	<u>0.037</u>	<u>40.60</u>	<u>0.974</u>	<u>0.034</u>	<u>41.42</u>	<u>0.977</u>	<u>0.031</u>
	SVDinsTN	36.48	0.939	0.054	<u>38.26</u>	<u>0.957</u>	<u>0.044</u>	39.03	0.963	0.041	40.33	0.970	0.035	41.40	0.976	<u>0.031</u>
	TenExp	38.97	0.961	0.044	39.83	0.967	0.037	40.94	0.973	0.032	41.57	0.976	0.030	42.05	0.978	0.028
<i>Akiyo</i> (144×176×3×30)	HaLRTC	18.39	0.576	0.263	24.97	0.762	0.123	27.62	0.829	0.091	29.12	0.864	0.076	30.54	0.892	0.065
	SiLRTCTT	29.49	0.876	0.073	32.41	0.922	0.052	34.85	0.946	0.040	36.32	0.960	0.033	37.70	0.969	0.028
	TRLRF	32.44	0.895	0.052	33.40	0.909	0.046	34.44	0.925	0.041	36.83	0.950	0.031	37.12	0.952	0.030
	HTNN	35.18	0.947	0.038	37.34	0.964	0.029	38.95	0.973	0.024	40.46	0.979	0.020	41.77	0.984	0.017
	LTNN	32.27	0.902	0.059	36.22	0.960	0.033	38.61	<u>0.973</u>	0.025	<u>40.69</u>	0.981	<u>0.020</u>	41.89	0.984	<u>0.017</u>
	SVDinsTN	<u>35.90</u>	0.945	<u>0.035</u>	<u>38.02</u>	0.962	<u>0.027</u>	38.73	0.967	0.025	40.33	0.977	0.021	<u>42.02</u>	0.983	<u>0.017</u>
	TenExp	37.32	0.957	0.029	39.21	0.969	0.024	40.99	0.977	0.019	41.95	0.981	0.017	43.12	0.984	0.015

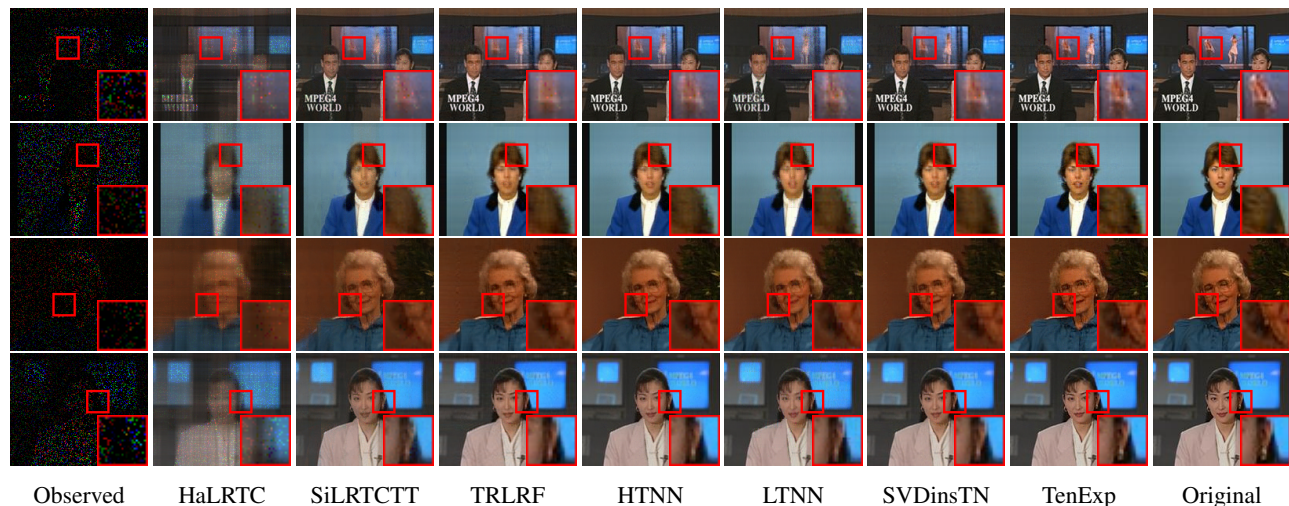


Fig. 4: The completion results of realistic color videos by different methods on *News*, *Claire*, *Grandma*, and *Akiyo* with SR = 0.1.

demonstrate comparable performance in most cases. Notably, SVDinsTN achieves the second-best or third-best performance across most MSIs, which can be attributed to its effective low-rank characterization of data. Importantly, the proposed TenExp significantly outperforms all other methods across all evaluation metrics. This superiority stems from its ability to deliver a suitable mixture of decompositions beyond a single decomposition.

Fig. 3 provides a visual comparison of the MSI completion results from all compared tensor decomposition-based methods. For enhanced clarity, the region of interest (marked by a

red rectangle) at the bottom-right corner of each image is enlarged. From the visual results, we can observe that HaLRTC effectively restores the primary outlines of missing regions but struggles with capturing fine-grained details and maintaining color fidelity. In contrast, SiLRTCTT, TRLRF, HTNN, and LTNN produce completion results with richer spatial details. However, their performance remains unsatisfactory in terms of local fine details. SVDinsTN yields visually pleasing results in both spatial geometry and color consistency, though subtle blurring artifacts are still observable. By comparison, our TenExp outperforms all other approaches in preserving both

TABLE VI: The quantitative results for realistic light field data completion by different methods. The **best** and second-best values are highlighted.

SR		0.1			0.15			0.2			0.25			0.3		
Data	Method	PSNR	SSIM	RE												
<i>Greek</i> (128×128×3×30)	HaLRTC	17.16	0.524	0.247	22.78	0.737	0.129	25.10	0.815	0.099	26.57	0.856	0.083	27.94	0.888	0.071
	SiLRTCCT	27.53	0.880	0.074	28.18	0.887	0.069	30.07	0.921	0.055	31.67	0.943	0.046	33.15	0.957	0.039
	TRLRF	24.37	0.715	0.107	28.70	0.869	0.065	29.05	0.876	0.062	29.41	0.887	0.060	29.76	0.890	0.057
	HTNN	29.06	0.890	0.062	31.07	0.927	0.049	32.95	0.950	0.040	34.67	0.965	0.032	36.39	0.975	0.027
	LTNN	29.37	0.909	0.060	32.28	0.952	0.043	34.86	0.972	0.032	36.85	0.982	0.025	38.62	0.987	0.020
	SVDinsTN	30.94	0.907	0.050	32.96	0.936	0.040	34.37	0.955	0.034	37.26	0.977	0.024	39.42	0.984	0.019
	TenExp	32.52	0.943	0.042	35.04	0.962	0.031	37.72	0.979	0.023	39.77	0.986	0.018	40.99	0.989	0.015
<i>Museum</i> (128×128×3×30)	HaLRTC	21.71	0.694	0.158	27.59	0.866	0.080	29.44	0.899	0.065	30.93	0.921	0.054	32.31	0.938	0.046
	SiLRTCCT	29.95	0.901	0.061	30.93	0.921	0.054	33.08	0.944	0.042	34.70	0.958	0.035	36.12	0.967	0.030
	TRLRF	29.35	0.847	0.065	33.32	0.926	0.041	34.88	0.942	0.034	35.64	0.950	0.031	36.92	0.961	0.027
	HTNN	35.08	0.955	0.034	36.90	0.968	0.027	38.47	0.977	0.022	39.89	0.983	0.019	41.22	0.987	0.016
	LTNN	32.60	0.939	0.045	36.77	0.972	0.027	39.53	0.983	0.020	41.62	0.989	0.016	44.46	0.994	0.011
	SVDinsTN	35.27	0.947	0.033	37.22	0.964	0.026	39.90	0.978	0.019	41.30	0.983	0.016	42.19	0.985	0.014
	TenExp	37.85	0.967	0.024	41.22	0.984	0.016	42.47	0.987	0.014	45.83	0.993	0.009	46.14	0.994	0.009
<i>Medieval2</i> (128×128×3×30)	HaLRTC	23.67	0.775	0.202	26.53	0.859	0.145	28.35	0.896	0.118	29.89	0.922	0.098	31.43	0.942	0.082
	SiLRTCCT	29.23	0.914	0.106	30.62	0.933	0.090	32.56	0.954	0.072	34.05	0.965	0.061	35.48	0.974	0.051
	TRLRF	29.09	0.892	0.108	31.79	0.937	0.079	33.72	0.960	0.063	35.35	0.971	0.052	36.78	0.979	0.044
	HTNN	33.95	0.966	0.061	35.57	0.976	0.051	37.00	0.982	0.043	38.26	0.986	0.037	39.47	0.989	0.032
	LTNN	32.76	0.958	0.071	37.63	0.987	0.040	40.48	0.992	0.029	42.25	0.995	0.023	43.74	0.996	0.020
	SVDinsTN	35.84	0.975	0.049	38.52	0.986	0.036	39.96	0.990	0.031	41.58	0.993	0.025	42.40	0.993	0.023
	TenExp	36.11	0.977	0.048	39.96	0.991	0.031	42.02	0.994	0.024	44.88	0.996	0.017	45.61	0.997	0.016
<i>Vinyl</i> (128×128×3×30)	HaLRTC	23.30	0.722	0.228	26.26	0.826	0.162	28.16	0.876	0.130	30.07	0.912	0.104	31.73	0.936	0.086
	SiLRTCCT	29.87	0.903	0.107	31.07	0.923	0.093	33.11	0.948	0.073	34.83	0.963	0.060	36.29	0.972	0.051
	TRLRF	26.86	0.787	0.151	31.63	0.903	0.087	33.27	0.934	0.072	34.59	0.947	0.062	38.45	0.975	0.039
	HTNN	34.68	0.958	0.061	36.80	0.973	0.048	38.52	0.982	0.039	40.16	0.987	0.032	41.59	0.990	0.027
	LTNN	32.99	0.946	0.074	39.60	0.986	0.034	42.62	0.993	0.024	44.70	0.995	0.019	46.24	0.996	0.016
	SVDinsTN	34.87	0.952	0.060	40.12	0.984	0.032	42.14	0.990	0.026	43.81	0.993	0.021	45.37	0.995	0.017
	TenExp	38.23	0.975	0.040	44.31	0.993	0.020	46.51	0.995	0.015	50.39	0.998	0.010	50.75	0.998	0.009

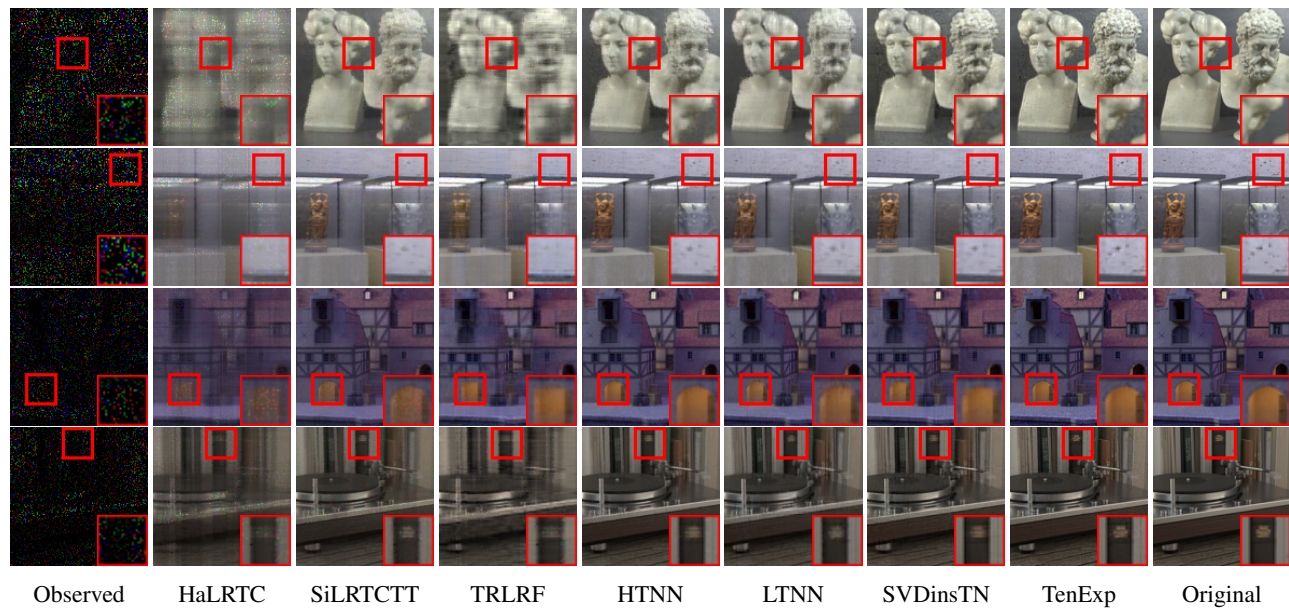


Fig. 5: The completion results of light field data by different methods on *Greek*, *Museum*, *Medieval2*, and *Vinyl* with SR = 0.1.

global structure and local details, which further validates its powerful recovery capability.

5) *Experimental Results of Color Videos*: Table V presents the quantitative metrics (PSNR, SSIM, and RE) of all competing methods for color video completion under various sampling rates. A comparison of these results reveals that our TenExp distinctly outperforms other baseline methods, achieving the optimal PSNR, SSIM, and RE values across

most experimental settings. Specifically, TenExp delivers a notable PSNR improvement of approximately 1–3 dB over the second-best performing methods (i.e., HTNN or LTNN).

Further visual validation of the performance of our method is provided in Fig. 4, which displays a representative frame from the reconstructed videos under the challenging SR=0.1 condition (i.e., 90% of data missing). The visual results strongly confirm the effectiveness of TenExp. Compared to other

baseline methods, the proposed TenExp significantly excels at accurately reconstructing both the global structural coherence of video frames and their intricate local details (e.g., texture and edge sharpness). This superiority directly stems from the powerful representation capability of the proposed TenExp, which leverages the adaptive mixture of decompositions to model the spatiotemporal correlations of video data.

6) *Experimental Results of Light Field Data*: Table VI provides a quantitative comparison of all compared methods for light field data completion under various sampling rates. For clarity, the best-performing results are highlighted in bold, and the second-best in underline. Notably, the proposed TenExp method consistently outperforms all competitors, achieving the optimal PSNR, SSIM, and RE values across all sampling rates. This consistent superiority underscores the effectiveness of TenExp in handling multi-dimensional data with complex structural dependencies and intricate textural details.

Additionally, Fig. 5 offers visual validation of the reconstruction quality for light field data under the stringent SR=0.1 condition. In this extreme scenario, where the high dimensionality and structural complexity of light field data pose significant challenges, the compared methods often exhibit pronounced limitations: reconstructed results suffer from distorted local details, loss of textural fidelity, or excessive smoothing artifacts. In sharp contrast, TenExp distinguishes itself by preserving fine textures and structural details. These visual results further validate its superior capability in processing complex light field data, aligning with the quantitative metrics in Table VI.

Overall, these results validate the innovative value of the TenExp, which provides a framework that not only can provide a suitable single decomposition beyond a fixed factor-interaction family but also can deliver a suitable mixture of decompositions beyond a single decomposition. These two unique advantages surpass the state-of-the-art tensor decomposition structure search methods.

VI. DISCUSSION

In this section, we discuss the influence of four aspects of the TenExp, i.e., the search capability, the candidate selection strategy, the parameters updating order, and the energy ratio threshold.

A. The Search Capability of the Proposed TenExp

To comprehensively evaluate the search capability of the TenExp, we present the PSNR values and corresponding tensor decomposition structures for the representative search method (i.e., SVDinsTN) and the proposed TenExp across various data with a sampling rate of 0.2. As presented in Table VII, TenExp demonstrates a superior capability to deliver a suitable tensor decomposition structure. Specifically, SVDinsTN can only search the tensor network decomposition under the tensor contraction family. In contrast, the proposed TenExp not only can provide a suitable single decomposition beyond a fixed factor-interaction family but also can deliver a suitable mixture of decompositions beyond a single decomposition, which yields higher PSNR values than SVDinsTN. Additionally, we can observe that increasing the top- k value enhances the

TABLE VII: The PSNR values and corresponding tensor factor-interaction families of the representative search method (i.e., SVDinsTN) and the proposed TenExp across various data with a sampling rate of 0.2. The symbol ‘+’ represents the mixture of decompositions.

	<i>Flowers</i>	<i>Beers</i>	<i>Balloons</i>	<i>Feathers</i>
Data				
SVDinsTN	Tensor Contraction	Tensor Contraction	Tensor Contraction	Tensor Contraction
	38.18	42.72	42.08	38.83
Top-1 TenExp	T-Product	Tensor Contraction	T-Product	T-Product
	42.51	46.42	42.87	41.54
Top-2 TenExp	Tensor Contraction+ T-Product	Tensor Contraction+ T-Product	Tensor Contraction+ T-Product	Tensor Contraction+ T-Product
	42.57	48.30	48.08	41.86
Top-3 TenExp	ALL	ALL	ALL	ALL
	42.70	48.79	49.49	42.54

performance, as it combines the unique advantages of different factor interactions; see Fig. 2.

TABLE VIII: The proposed TenExp variants with different candidate selection strategies for MSIs *Flowers*, *Balloons*, and *Feathers* with a sampling rate of 0.2.

Data	<i>Flowers</i>		<i>Balloons</i>		<i>Feathers</i>	
Selection Strategy	PSNR	SSIM	PSNR	SSIM	PSNR	SSIM
Max Sampling	42.51	0.985	49.49	0.996	41.54	0.980
Random Sampling	37.64	0.880	40.70	0.973	37.97	0.949

B. The Influence of the Candidate Selection Strategy

To analyze the influence of candidate selection strategy on the proposed TenExp, we illustrate the performance (in terms of PSNR and SSIM) of TenExp variants with different candidate selection strategies (i.e., max sampling and random sampling) for MSIs *Flowers*, *Balloons*, and *Feathers* with a sampling rate of 0.2 in Table VIII. The max sampling strategy (selecting one candidate tensor decomposition with the highest gating value) consistently outperforms the random sampling strategy (randomly selecting one candidate tensor decomposition based on their predicted gating values) across all data. Thus, in our experiments, we adopt the max sampling strategy as the candidate selection strategy.

C. The Influence of the Parameters Updating Order

To discuss the influence of the parameters updating order, we present the performance of TenExp variants with different parameters updating orders for MSIs *Flowers*, *Balloons*, and *Feathers* with a sampling rate of 0.2 in Table IX. The notations in the table are defined as

TABLE IX: The proposed TenExp variants with different parameters updating orders for MSIs *Flowers*, *Balloons*, and *Feathers* with a sampling rate of 0.2.

Data	<i>Flowers</i>		<i>Balloons</i>		<i>Feathers</i>	
Updating Order	PSNR	SSIM	PSNR	SSIM	PSNR	SSIM
I	42.99	0.938	46.76	0.994	41.65	0.981
II	42.70	0.939	49.49	0.996	42.54	0.984
III	34.34	0.895	41.63	0.983	35.94	0.941

- Order I: Simultaneous update of all candidate tensor decompositions and all gating values.
- Order II: Alternating updates between all candidate tensor decompositions and all gating values.
- Order III: Alternating updates between each individual candidate tensor decomposition and its corresponding gating value.

From Table IX, we can observe that updating order II consistently outperforms the other two updating orders across all data. The success of updating order II lies in its capability to balance the need for joint optimization between candidate tensor decompositions and gating values while allowing for iterative refinement through alternation, thus leveraging the synergies between these components to achieve enhanced reconstruction performance.

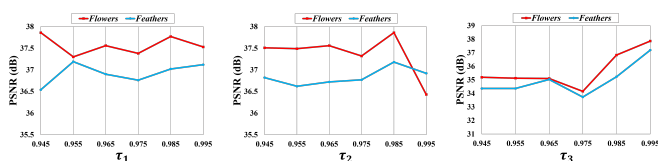


Fig. 6: The PSNR values of the proposed TenExp with different values of energy ratio thresholds for MSIs *Flowers* and *Feathers* with a sampling rate of 0.1.

D. The Influence of the Energy Ratio Threshold

Choosing appropriate energy ratio thresholds is a crucial step in the proposed TenExp. To comprehensively examine the influence of energy ratio thresholds on the performance of the proposed TenExp, we modify the value of one energy ratio threshold at a time while fixing the others. The results are presented in Fig. 6. From these results, we find that our method shows a certain degree of robustness, given its ability to achieve satisfactory performance across a wide range of values.

VII. CONCLUSION

In this work, to address the challenging and relatively under-explored problem of selecting a suitable tensor decomposition to exactly capture the low-rank structures behind the data, we elaborately designed a mixture-of-experts-based tensor decomposition structure search framework, which allows us to dynamically select and activate suitable tensor decompositions in an unsupervised fashion. This framework enjoys two unique

advantages over the state-of-the-art tensor decomposition structure search methods. Firstly, TenExp can provide a suitable single decomposition beyond a fixed factor-interaction family. Secondly, TenExp can deliver a suitable mixture of decompositions beyond a single decomposition. Theoretically, we also provided the approximation error bound of TenExp, which reveals the approximation capability of TenExp. To evaluate the effectiveness of the proposed TenExp, we proposed an unsupervised TenExp-based multi-dimensional data recovery model. Extensive experiments on both synthetic and realistic datasets demonstrated the superiority of the proposed TenExp over the state-of-the-art tensor decomposition-based methods.

REFERENCES

- [1] X. Chen, D. Zhuang, H. Cai, S. Wang, and J. Zhao, “Dynamic autoregressive tensor factorization for pattern discovery of spatiotemporal systems,” *IEEE Transactions on Pattern Analysis and Machine Intelligence*, vol. 47, no. 10, pp. 8524–8537, 2025.
- [2] X. Chen and L. Sun, “Bayesian temporal factorization for multidimensional time series prediction,” *IEEE Transactions on Pattern Analysis and Machine Intelligence*, vol. 44, no. 9, pp. 4659–4673, 2022.
- [3] H. Wang, J. Peng, W. Qin, J. Wang, and D. Meng, “Guaranteed tensor recovery fused low-rankness and smoothness,” *IEEE Transactions on Pattern Analysis and Machine Intelligence*, vol. 45, no. 9, pp. 10990–11007, 2023.
- [4] Q. Xie, Q. Zhao, D. Meng, and Z. Xu, “Kronecker-basis-representation based tensor sparsity and its applications to tensor recovery,” *IEEE Transactions on Pattern Analysis and Machine Intelligence*, vol. 40, no. 8, pp. 1888–1902, 2018.
- [5] X. Zhang and M. K. Ng, “Low rank tensor completion with poisson observations,” *IEEE Transactions on Pattern Analysis and Machine Intelligence*, vol. 44, no. 8, pp. 4239–4251, 2022.
- [6] W. He, Q. Yao, C. Li, N. Yokoya, Q. Zhao, H. Zhang, and L. Zhang, “Non-local meets global: An iterative paradigm for hyperspectral image restoration,” *IEEE Transactions on Pattern Analysis and Machine Intelligence*, vol. 44, no. 4, pp. 2089–2107, 2022.
- [7] K. Han and W. Xiang, “Multiscale tensor decomposition and rendering equation encoding for view synthesis,” in *Proceedings of the IEEE/CVF Conference on Computer Vision and Pattern Recognition*, 2023, pp. 4232–4241.
- [8] P. Rai, Y. Wang, S. Guo, G. Chen, D. Dunson, and L. Carin, “Scalable bayesian low-rank decomposition of incomplete multiway tensors,” in *Proceedings of the International Conference on Machine Learning*, vol. 32, 2014.
- [9] Q. Zhao, L. Zhang, and A. Cichocki, “Bayesian cp factorization of incomplete tensors with automatic rank determination,” *IEEE Transactions on Pattern Analysis and Machine Intelligence*, vol. 37, pp. 1751–1763, 2014.
- [10] A. Cichocki, N. Lee, I. Oseledets, A.-H. Phan, Q. Zhao, and D. P. Mandic, “Tensor networks for dimensionality reduction and large-scale optimization: Part I low-rank tensor decompositions,” *Foundations And Trends In Machine Learning*, vol. 9, no. 4–5, p. 249–429, 2016.
- [11] M. Shakeri and H. Zhang, “Moving object detection under discontinuous change in illumination using tensor low-rank and invariant sparse decomposition,” in *Proceedings of the IEEE/CVF Conference on Computer Vision and Pattern Recognition*, 2019, pp. 7214–7223.
- [12] Y. Luo, X. Zhao, D. Meng, and T. Jiang, “HLRTF: Hierarchical low-rank tensor factorization for inverse problems in multi-dimensional imaging,” in *Proceedings of the IEEE/CVF Conference on Computer Vision and Pattern Recognition*, 2022, pp. 19281–19290.
- [13] R. Yamamoto, H. Hontani, A. Imakura, and T. Yokota, “Fast algorithm for low-rank tensor completion in delay-embedded space,” in *Proceedings of the IEEE/CVF Conference on Computer Vision and Pattern Recognition*, 2022, pp. 2048–2056.
- [14] X. Zhang, X. Yuan, and L. Carin, “Nonlocal low-rank tensor factor analysis for image restoration,” in *Proceedings of the IEEE/CVF Conference on Computer Vision and Pattern Recognition*, 2018, pp. 8232–8241.
- [15] F. L. Hitchcock, “The expression of a tensor or a polyadic as a sum of products,” *Journal of Mathematics and Physics*, vol. 6, no. 1–4, pp. 164–189, 1927.

- [16] L. R. Tucker, "Some mathematical notes on three-mode factor analysis," *Psychometrika*, vol. 31, no. 3, pp. 279–311, 1966.
- [17] C. Li and Z. Sun, "Evolutionary topology search for tensor network decomposition," in *Proceedings of the International Conference on Machine Learning*, vol. 119, 2020, p. 5947–5957.
- [18] M. E. Kilmer, K. Braman, N. Hao, and R. C. Hoover, "Third-order tensors as operators on matrices: A theoretical and computational framework with applications in imaging," *SIAM Journal on Matrix Analysis and Applications*, vol. 34, no. 1, pp. 148–172, 2013.
- [19] N. D. Sidiropoulos, L. De Lathauwer, X. Fu, K. Huang, E. E. Papalexakis, and C. Faloutsos, "Tensor decomposition for signal processing and machine learning," *IEEE Transactions on Signal Processing*, vol. 65, no. 13, pp. 3551–3582, 2017.
- [20] Z. Chen, Z. Xu, and D. Wang, "Deep transfer tensor decomposition with orthogonal constraint for recommender systems," in *Proceedings of the AAAI Conference on Artificial Intelligence*, vol. 35, no. 5, 2021, pp. 4010–4018.
- [21] J.-T. Chien and Y.-T. Bao, "Tensor-factorized neural networks," *IEEE Transactions on Neural Networks and Learning Systems*, vol. 29, no. 5, pp. 1998–2011, 2018.
- [22] I. V. Oseledets, "Tensor-train decomposition," *SIAM Journal on Scientific Computing*, vol. 33, no. 5, pp. 2295–2317, 2011.
- [23] Q. Zhao, G. Zhou, S. Xie, L. Zhang, and A. Cichocki, "Tensor ring decomposition," *ArXiv*, vol. abs/1606.05535, 2016.
- [24] Y.-B. Zheng, T.-Z. Huang, X.-L. Zhao, Q. Zhao, and T.-X. Jiang, "Fully-connected tensor network decomposition and its application to higher-order tensor completion," in *Proceedings of the AAAI Conference on Artificial Intelligence*, vol. 35, no. 12, 2021, pp. 11 071–11 078.
- [25] L. Xu, L. Cheng, N. Wong, and Y.-C. Wu, "To fold or not to fold: Graph regularized tensor train for visual data completion," *IEEE Transactions on Pattern Analysis and Machine Intelligence*, pp. 1–18, 2025.
- [26] J. A. Bengua, H. N. Phien, H. D. Tuan, and M. N. Do, "Efficient tensor completion for color image and video recovery: Low-rank tensor train," *IEEE Transactions on Image Processing*, vol. 26, no. 5, pp. 2466–2479, 2017.
- [27] W. Wang, V. Aggarwal, and S. Aeron, "Efficient low rank tensor ring completion," in *Proceedings of the IEEE International Conference on Computer Vision*, 2017, pp. 5698–5706.
- [28] Z.-L. Han, T.-Z. Huang, X.-L. Zhao, H. Zhang, and W.-H. Wu, "Nested fully-connected tensor network decomposition for multi-dimensional visual data recovery," *IEEE Transactions on Circuits and Systems for Video Technology*, vol. 34, no. 10, pp. 10 092–10 106, 2024.
- [29] Y. Zhou and Y.-M. Cheung, "Bayesian low-tubal-rank robust tensor factorization with multi-rank determination," *IEEE Transactions on Pattern Analysis and Machine Intelligence*, vol. 43, no. 1, pp. 62–76, 2021.
- [30] J. Hou, F. Zhang, H. Qiu, J. Wang, Y. Wang, and D. Meng, "Robust low-tubal-rank tensor recovery from binary measurements," *IEEE Transactions on Pattern Analysis and Machine Intelligence*, vol. 44, no. 8, pp. 4355–4373, 2022.
- [31] F. Zhang, J. Wang, W. Wang, and C. Xu, "Low-tubal-rank plus sparse tensor recovery with prior subspace information," *IEEE Transactions on Pattern Analysis and Machine Intelligence*, vol. 43, no. 10, pp. 3492–3507, 2021.
- [32] S. Liu, X.-L. Zhao, J. Leng, B.-Z. Li, J.-H. Yang, and X. Chen, "Revisiting high-order tensor singular value decomposition from basic element perspective," *IEEE Transactions on Signal Processing*, vol. 72, pp. 4589–4603, 2024.
- [33] M. Ghadiri, M. Fahrback, G. Fu, and V. Mirrokni, "Approximately optimal core shapes for tensor decompositions," in *Proceedings of the International Conference on Machine Learning*, no. 451, 2023, pp. 11 237 – 11 254.
- [34] M. Hashemizadeh, M. Liu, J. Miller, and G. Rabusseau, "Adaptive learning of tensor network structures," *ArXiv*, vol. abs/2008.05437, 2020.
- [35] C. Li, J. Zeng, Z. Tao, and Q. Zhao, "Permutation search of tensor network structures via local sampling," in *Proceedings of the International Conference on Machine Learning*, vol. 162, 2022, pp. 13 106–13 124.
- [36] C. Li, J. Zeng, C. Li, C. F. Caiafa, and Q. Zhao, "Alternating local enumeration (TnALE): Solving tensor network structure search with fewer evaluations," in *Proceedings of the International Conference on Machine Learning*, vol. 202, 2023, pp. 20 384–20 411.
- [37] N. Li, Y. Pan, Y. Chen, Z. Ding, D. Zhao, and Z. Xu, "Heuristic rank selection with progressively searching tensor ring network," *Complex & Intelligent Systems*, vol. 8, p. 771–785, 2022.
- [38] Y. Liu, J. Chen, Y. Lu, W. Ou, Z. Long, and C. Zhu, "Adaptively topological tensor network for multi-view subspace clustering," *IEEE Transactions on Knowledge and Data Engineering*, vol. 36, no. 11, p. 5562–5575, 2024.
- [39] C. Nie, H. Wang, and L. Tian, "Adaptive tensor networks decomposition," in *Proceedings of the British Machine Vision Conference*, 2021, p. 148.
- [40] F. Sedighin, A. Cichocki, and A.-H. Phan, "Adaptive rank selection for tensor ring decomposition," *IEEE Journal of Selected Topics in Signal Processing*, vol. 15, no. 3, pp. 454–463, 2021.
- [41] Y.-B. Zheng, X.-L. Zhao, J. Zeng, C. Li, Q. Zhao, H. C. Li, and T.-Z. Huang, "SVDinsTN: A tensor network paradigm for efficient structure search from regularized modeling perspective," in *Proceedings of the IEEE/CVF Conference on Computer Vision and Pattern Recognition*, 2024, pp. 22 413–22 422.
- [42] T. G. Kolda and B. W. Bader, "Tensor decompositions and applications," *SIAM Review*, vol. 51, no. 3, pp. 455–500, 2009.
- [43] M. E. Kilmer, L. Horesh, H. Avron, and E. Newman, "Tensor-tensor algebra for optimal representation and compression of multiway data," *Proceedings of the National Academy of Sciences of the United States of America*, vol. 118, no. 28, p. e2015851118, 2021.
- [44] Y.-B. Zheng, X.-L. Zhao, H.-C. Li, C. Li, T.-Z. Huang, and Q. Zhao, "Tensor network decomposition for data recovery: Recent advancements and future prospects," *Neural Networks*, vol. 191, p. 107808, 2025.
- [45] P. Zhou, C. Lu, Z. Lin, and C. Zhang, "Tensor factorization for low-rank tensor completion," *IEEE Transactions on Image Processing*, vol. 27, no. 3, pp. 1152–1163, 2018.
- [46] D. P. Kingma and J. Ba, "Adam: A method for stochastic optimization," *ArXiv*, vol. abs/1412.6980, 2014.
- [47] J. Liu, P. Musialski, P. Wonka, and J. Ye, "Tensor completion for estimating missing values in visual data," *IEEE Transactions on Pattern Analysis and Machine Intelligence*, vol. 35, no. 1, p. 208–220, 2013.
- [48] L. Yuan, C. Li, D. Mandic, J. Cao, and Q. Zhao, "Tensor ring decomposition with rank minimization on latent space: an efficient approach for tensor completion," in *Proceedings of the AAAI Conference on Artificial Intelligence*, 2019.
- [49] W. Qin, H. Wang, F. Zhang, J. Wang, X. Luo, and T. Huang, "Low-rank high-order tensor completion with applications in visual data," *IEEE Transactions on Image Processing*, vol. 31, pp. 2433–2448, 2022.
- [50] Y. Qiu, G. Zhou, A. Wang, Q. Zhao, and S. Xie, "Balanced unfolding induced tensor nuclear norms for high-order tensor completion," *IEEE Transactions on Neural Networks and Learning Systems*, vol. 36, no. 3, pp. 4724–4737, 2025.



Ting-Wei Zhou received the B.S. degree from the College of Science, Zhejiang University of Technology, Hangzhou, China, in 2023. He is currently pursuing the Ph.D. degree with the School of Mathematical Sciences, University of Electronic Science and Technology of China, Chengdu, China.

His research interests include high-order tensor modeling, computer vision, and unsupervised learning.



Xi-Le Zhao received the M.S. and Ph.D. degrees from the University of Electronic Science and Technology of China (UESTC), Chengdu, China, in 2009 and 2012. He worked as a post-doc with Prof. M. Ng at Hong Kong Baptist University from 2013 to 2014. He worked as a visiting scholar with Prof. J. Bioucas Dias at University of Lisbon from 2016 to 2017.

He is currently a Professor with the School of Mathematical Sciences, UESTC. His research interests include image processing, machine learning,

and scientific computing. More information can be found on his homepage <https://zhaoxile.github.io/>.



Sheng Liu received the B.S. degree in information and computer science from the Northwest A&F University, Yangling, China, in 2022. He is currently working toward the Ph.D. degree with the School of Mathematical Sciences, University of Electronic Science and Technology of China (UESTC), Chengdu, China.

His research interests include tensor modeling and algorithms for high-order data recovery.



Wei-Hao Wu received the B.S. degree from the School of Mathematical Sciences, University of Electronic Science and Technology of China, Chengdu, China, in 2021, where he is currently pursuing the Ph.D. degree.

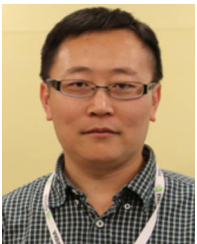
His research interests include model-based tensor modeling and unsupervised learning for low-level visual tasks, such as inpainting and denoising.



Yu-Bang Zheng received the B.S. degree from the Institute of Statistics and Applied Mathematics, Anhui University of Finance and Economics, Bengbu, China, in 2017, and the Ph.D. degree from the School of Mathematical Sciences, University of Electronic Science and Technology of China, Chengdu, China, in 2022. From 2021 to 2022, he was a Student Trainee with the Tensor Learning Team, RIKEN Center for Advanced Intelligence Project, Tokyo, Japan. He is currently an Assistant Professor with the School of Information Science and Technology, Southwest

Jiaotong University, Chengdu.

His current research interests include tensor modeling and computing, machine learning, and high-dimensional data processing.



Deyu Meng received the B.Sc., M.Sc., and Ph.D. degrees from Xi'an Jiaotong University, Xi'an, China, in 2001, 2004, and 2008, respectively.

He is currently a Professor with the School of Mathematics and Statistics, Xi'an Jiaotong University, and an Adjunct Professor with the Faculty of Information Technology, Macau University of Science and Technology, Macau, China. His research interests include model-based deep learning, variational networks, and meta-learning.

Dr. Meng currently serves as an Associate Editor for *IEEE Transactions on Pattern Analysis and Machine Intelligence*, *Science China-Information Sciences*, and *Frontiers of Computer Science*.